NASA TM-2012-217361

Evaluating Shielding Approaches to Reduce Space Radiation Cancer Risks

Francis A. Cucinotta
NASA Lyndon B. Johnson Space Center
Houston, Texas

Myung-Hee Y. Kim
U.S.R.A., Division of Space Life Sciences
Houston, Texas

Lori J. Chappell
U.S.R.A., Division of Space Life Sciences
Houston, Texas

May 2012

THE NASA STI PROGRAM OFFICE . . . IN PROFILE

Since its founding, NASA has been dedicated to the advancement of aeronautics and space science. The NASA Scientific and Technical Information (STI) Program Office plays a key part in helping NASA maintain this important role.

The NASA STI Program Office is operated by Langley Research Center, the lead center for NASA's scientific and technical information. The NASA STI Program Office provides access to the NASA STI Database, the largest collection of aeronautical and space science STI in the world. The Program Office is also NASA's institutional mechanism for disseminating the results of its research and development activities. These results are published by NASA in the NASA STI Report Series, which includes the following report types:

- TECHNICAL PUBLICATION. Reports of completed research or a major significant phase of research that present the results of NASA programs and include extensive data or theoretical analysis. Includes compilations of significant scientific and technical data and information deemed to be of continuing reference value. NASA's counterpart of peer-reviewed formal professional papers but has less stringent limitations on manuscript length and extent of graphic presentations.

- TECHNICAL MEMORANDUM. Scientific and technical findings that are preliminary or of specialized interest, e.g., quick release reports, working papers, and bibliographies that contain minimal annotation. Does not contain extensive analysis.

- CONTRACTOR REPORT. Scientific and technical findings by NASA-sponsored contractors and grantees.

- CONFERENCE PUBLICATION. Collected papers from scientific and technical conferences, symposia, seminars, or other meetings sponsored or cosponsored by NASA.

- SPECIAL PUBLICATION. Scientific, technical, or historical information from NASA programs, projects, and mission, often concerned with subjects having substantial public interest.

- TECHNICAL TRANSLATION. English-language translations of foreign scientific and technical material pertinent to NASA's mission.

Specialized services that complement the STI Program Office's diverse offerings include creating custom thesauri, building customized databases, organizing and publishing research results . . . even providing videos.

For more information about the NASA STI Program Office, see the following:

- Access the NASA STI Program Home Page at http://www.sti.nasa.gov

- E-mail your question via the Internet to help@sti.nasa.gov

- Fax your question to the NASA Access Help Desk at (301) 621-0134

- Telephone the NASA Access Help Desk at (301) 621-0390

- Write to:
  NASA Access Help Desk
  NASA Center for AeroSpace Information
  7121 Standard
  Hanover, MD 21076-1320

NASA TM-2012-217361

Evaluating Shielding Approaches to Reduce Space Radiation Cancer Risks

Francis A. Cucinotta
NASA Lyndon B. Johnson Space Center
Houston, Texas

Myung-Hee Y. Kim
U.S.R.A., Division of Space Life Sciences
Houston, Texas

Lori J. Chappell
U.S.R.A., Division of Space Life Sciences
Houston, Texas

May 2012

Available from:

NASA Center for AeroSpace Information
7121 Standard Drive
Hanover, MD 21076-1320

National Technical Information Service
5285 Port Royal Road
Springfield, VA 22161

This report is also available in electronic form at http://ston.jsc.nasa.gov/collections/TRS

Contents

Acronyms and Nomenclature

ALARA	as low as reasonably achievable
BEIR	(NAS) Committee on the Biological Effects of Ionizing Radiation
BRYNTRN	baryon transport computer code
CAMERA	computerized anatomical man model
CDC	Centers for Disease Control and Prevention
CDF	Cumulative Distribution Function
CI	confidence intervals
CL	confidence level
DDREF	dose and dose-rate reduction effectiveness factor
D_r	dose-rate (Gy/hr)
EAR	excess additive risk, Sv^{-1}
ERR	excess relative risk, Sv^{-1} yr^{-1}
EVA	extravehicular activity
F	fluence (number of ions per unit area) no. ions/cm^2
FS	former smokers
GCR	galactic cosmic ray
GM	geometric mean
GSD	geometric standard deviation
HZE	high charge and energy
HZETRN	high charge and energy transport computer code
ICRP	International Commission on Radiological Protection
ISS	International Space Station
KS	Kolmogorov-Smirnov
LEO	low Earth orbit
LET	linear energy transfer
LSS	Life-Span Study of the Japanese atomic-bomb survivors
NAS	National Academy of Sciences
NCRP	National Council on Radiation Protection and Measurements
NS	never-smokers
NTE	non-targeted effects
PDF	probability distribution function
Q	quality factor
Q(L)	quality factor as a function of linear energy transfer
$Q_{leukemia}$	quality factor for estimating leukemia risks
Q_{solid}	quality factor for estimating solid cancer risks
QMSFRG	quantum multiple scattering fragmentation
RBE	relative biological effectiveness
RBE_{max}	maximum relative biological effectiveness that assumes linear responses at low doses or dose-rates

REIC	risk of exposure-induced cancer incidence
REID	risk of exposure-induced death
RR	relative risks
S	smokers
SEER	surveillance, epidemiology, and end results
SPE	solar particle event
w_T	Tissue weighting factor
x_{Tr}	track structure scaling parameter equivalent to Z^*/β^2
x_α	quantiles (random variables) associated with factor α
UNSCEAR	United Nations Special Committee on the Effects of Atomic Radiation
Z	Charge number
Z^*	Effective charge number
α	Coefficient of linear dose response term, Gy^{-1}
β	Coefficient of quadratic dose-response term, Gy^{-2}
χ	Chi statistical test
$\phi_j(x,E)$	number of particles of type j with energy, E at depth, x in shielding, 1/(MeV/u cm^2)
λ_I	gender and age-specific cancer incidence rate, cancers/yr
λ_M	gender and age-specific cancer mortality rate, cancer deaths/yr
κ	Parameter in action cross section to determine most biologically effects Z^{*2}/β^2
σ	Action cross section or probability of effect per unit fluence, μm^2
Σ	Track structure derived risk cross section, μm^2

Abstract

It remains an important challenge for NASA to protect astronauts from galactic cosmic rays (GCRs) and solar particle events (SPEs) during long-duration space missions. Shielding of SPEs is well understood scientifically, which has led to readily available technology solutions, with optimization of specific designs to minimize launch mass—an important goal for risk assessment. However, the high-energies and secondary radiation of the GCR limit most shielding approaches to small reductions from a baseline shielding configuration. The larger uncertainties complicate understanding the effectiveness of potential mitigators, and in performing cost-benefit analysis required by the as low as reasonably achievable (ALARA) principle. Previously, we had shown that the knowledge to estimate the performance of different shielding materials was limited by the large uncertainties in the radiobiology of high charge and energy (HZE) nuclei. In this report, we make a revised assessment of shielding materials performance based on newly defined NASA track structure dependent radiation quality factors, and the most recent uncertainty analysis of space radiation cancer risks. Comparisons of liquid hydrogen, polyethylene, water, and epoxy shielding to aluminum for one-layer configurations with depths of 5 to 40 g/cm^2, or two-layer configurations with an outer 10 g/cm^2 aluminum layer, are considered. We show that statistically significant improvements in GCR risk reduction relative to aluminum shielding can be obtained with hydrocarbon materials with significant hydrogen content. These results demonstrate the important value to NASA of radiobiology research, which is the principal mechanism to reduce uncertainties. Comparisons for several spacecraft designs for solar minimum and solar maximum space radiation environments are discussed. Liquid hydrogen remains the optimal shielding material; however, its performance can be overestimated if secondary radiation produced in tissue or the vessel containing the hydrogen are not considered. Nevertheless, developing new multifunctional shielding materials with higher hydrogen content compared to polyethylene is advocated.

1.0 Introduction

In this report, we describe methods to evaluate spacecraft shielding effectiveness based on well-defined criteria using probabilistic models of space radiation cancer risks. Exposures to astronauts from GCRs made up of high-energy protons and high charge and energy (HZE) nuclei, and solar particle events (SPEs) comprised largely of low- to medium-energy protons, are a critical challenge for space exploration. Experimental studies have shown that HZE nuclei produce both qualitative and quantitative differences in biological effects compared to terrestrial radiation (NAS, 1996; Cucinotta and Durante, 2006; Durante and Cucinotta, 2008; Schimmerling *et al*., 1999; NCRP [National Council on Radiation Protection and Measurement], 2006) leading to large uncertainties in predicting exposure outcomes to human beings. NASA limits astronaut exposures to a 3% risk of exposure-induced death (REID) and protects against uncertainties in risks projections using an assessment of 95% confidence intervals (CI) in the projection model. The uncertainties in estimating the health risks from GCRs are a major limitation to the length of space missions and the evaluation of potential risk mitigations such as radiation shielding or biological countermeasures.

SPE shielding problems are readily solved by existing technologies, yet they require that optimization analysis to reduce mass and ensure other material requirements for spacecraft structures are satisfied. However, it is unlikely that there can be a technology solution to GCR risk from a shielding approach because of their high energies and limitations due to very high costs to launch large masses of shielding materials. In addition, active shielding devices require significant power sources or are exceptionally massive to achieve significant GCR risk reduction (Durante and Cucinotta, 2011). Material selection and optimization of topology are major considerations for both GCR and SPE. Spacecraft volumes may be constrained when considering shielding retrofits or design augmentations, which further complicates shielding approaches. More importantly, the extra fuel required to launch such shielding compounds the mass dedicated to shielding. Also, a competition exists between shielding mass relative to other necessary resources or flight safety factors. Dual-use shielding approaches, such as water, fuel, and food stowage, are useful in this regard. In-situ shielding using planetary resources is also of interest. Previously, we had shown that the large uncertainties in radiobiology knowledge limit NASA's ability to judge shielding performance (Cucinotta *et al*., 2006). In this report, we apply NASA's latest assessment tools for cancer risk and uncertainty factors to reevaluate shielding material performance.

2.0 Basic Concepts in Radiation Protection and Shielding

Radiation exposures are often described in terms of the physical quantity absorbed dose, D, which is defined as the energy deposited per unit mass. Dose has units of Joule/kg, which defines the special unit, 1 Gray (Gy), which is equivalent to 100 rad (0.01 Gy= 1 rad). In space, each cell within an astronaut is exposed every few days to a nuclear particle, which comprise the GCRs (Cucinotta *et al*., 1998). GCRs are the nuclei of atoms accelerated to high energies

where the atomic electrons are stripped off. It is common to discuss the number of particles per unit area, called the fluence, *F,* with units of $1/cm^2$. As particles pass through matter, they lose energy at a rate dependent on their kinetic energy, *E*, and charge number, *Z*, and approximately the average ratio of charge to mass (Z_T/A_T) of the materials they traverse. The rate of energy loss is called the linear energy transfer (LET), which for unit density materials such as tissue is given in units of keV/μm. The dose and fluence are related by $D = \rho F LET$, where ρ is the density of the material (e.g., 1 g/cm^3 for water or tissue). A broad energy range for the cosmic rays and the spectra of particles is denoted as the fluence spectra, $\phi_j(E)$, where *j* refers to the particle type described by *Z* and the mass number, *A*. Related to the kinetic energy is the particle velocity scaled to the speed of light denoted as β. Using relativistic kinematics, *E* and β are related using the formula $\gamma = 1 + E/m$ where *m* is the nucleon rest mass (938 MeV), and $\beta = (1 - 1/\gamma^2)^{-1/2}$. Kinetic energies are often expressed in units of MeV per atomic mass unit (u), MeV/u because particles with identical E then have the same β. The total kinetic energy of the particle is then *A* times *E*.

2.1 Shielding of Galactic Cosmic Rays

The GCRs of interest have charge number, *Z* from 1 to 28, and energy from less than 1 MeV/u to more than 10,000 MeV/u with a median energy of about 1,000 MeV/u. The GCRs with energies less than about 2,000 MeV/u are modulated by the 11-year solar cycle, with more than two-times higher GCR flux at solar minimum when the solar wind is weakest compared to the flux at solar maximum. The most recent solar minimum was in 2008-2009, and the next will occur in 2019-2020. Engineering considerations on material strength, temperature, ultraviolet degradation, flammability, etc., must be considered alongside of radiation protection, and the composite picture must be analyzed. Materials with the smallest mean atomic mass are usually the most efficient shields for both SPE and GCR, as described next. The composition of the radiation field changes as particles lose energy and suffer nuclear interactions in traversing structural materials, instruments, and the tissues of astronauts. Both the energy loss and the changes in particle fluence are related to the number of atoms per unit mass (in units such as grams) in the traversed material, which, in turn, is proportional to Avogadro's number divided by the atomic mass number, A_T, for each element of the material. The energy loss by ionization of a single component of shielding material with atomic number Z_T is proportional to the number of electrons per atom and thus proportional to Z_T/A_T. However, the energy lost per gram of material and per incident fluence (e.g., in units of particles per cm^2), the "mass stopping power," is also inversely proportional to the density, ρ (e.g., in g/cm^3) of the material, so that the energy lost by one incident particle per cm^2 per unit mass is proportional to $Z/\rho A$.

The number of nuclear interactions per unit mass and per unit incident fluence is proportional to σ/A, where σ is the total nuclear reaction cross section (Wilson *et al.,* 1991; 1995). To a first approximation, σ is proportional to $A^{2/3}$, so that the nuclear transmission is proportional to $1/A^{1/3}$. The ratio of electronic stopping power to nuclear interaction transmission is therefore proportional to $Z/\rho\ A^{2/3}$. Materials with small atomic mass have the highest number of electrons per nucleon (e.g., Z/A is 1 for hydrogen, 0.5 for carbon, 0.48 for aluminum, 0.46 for iron, and 0.40 for lead). Light mass materials have smaller nuclei and therefore more of them can fit into a

given mass so that there can be more nuclear interactions. Furthermore, the ratio of ionization energy loss to nuclear interactions is also dependent on the material density. For liquid hydrogen (ρ =0.07 g/cm^3), the ratio is approximately 14, whereas for aluminum (ρ =2.7 g/cm^3) the ratio is only 0.5, and for lead (ρ =11.3 g/cm^3) the ratio is 0.2 (Wilson *et al*., 1991). Thus, an electron plasma would provide the best shield from GCRs. A shield made of liquid hydrogen, which has the highest ratio of electrons to nuclei per atom and produce minimal secondary radiation (e.g., mesons), is the second-best choice. Hence, interest in polyethylene and hydrogen embedded nanofibers.

The character of particle interactions and the secondary nuclei produced through both projectile and target fragmentation is important in shielding considerations. Lighter nuclei have fewer neutrons to release and some nuclei (e.g., carbon) can break into three helium nuclei without releasing any neutrons (Cucinotta and Dubey, 1994). In tissue, the release of three helium atoms is much more biologically damaging than that of neutrons; however, if produced within spacecraft shielding materials, neutrons are a higher concern because of their longer ranges than slow helium particles. For very thick shields, lighter nuclei are also more effective in shielding against the built-up neutrons. For these and related reasons, detailed knowledge of the actual composition of the radiation fields (and of the biological consequences of exposure to them) is required to evaluate the net effect of shielding materials.

Energy loss by cosmic rays is through ionization and excitation of target atoms in the shielding material or tissue. The ionization of atoms leads to the liberation of electrons that often have sufficient energy to cause further excitations and ionizations of nearby target atoms. These electrons are called δ-rays and can have energies more than 1 MeV for ions with E >1,000 MeV/u. For HZE particles, about 80% of a particle's LET is due to ionizations leading to δ-rays (Cucinotta *et al*., 1999). The number of δ-rays created is proportional to Z^{*2}/β^2, where Z* is the effective charge number that adjusts Z by atomic screening effects important at low *E* and high *Z*. The lateral spread of δ-rays is called the track-width (illustrated in **Figure 1**) of the particle, and dependent on β but not Z, being determined by kinematics. At 1 MeV/u, the track-width is about 100 nm (0.1 μm) and at 1000 MeV/u the track-width is about 1 cm. A phenomenological approach to describing atomic ionization and excitation is to introduce an empirical model of energy deposition. To apply the model, some definition of a characteristic target volume is needed. A diverse choice of volumes are used in radiobiology, including ones with diameters <10 nm to represent short DNA segments, and of diameters from a few to 10 microns to represent cell nuclei or cells. Energy deposition is the sum of the energy transfer events due to ionizations and excitations in the volume, including those from δ-rays. For large target volumes, energy deposition and energy loss (LET) become approximately the same. Two particles with different *Z* and identical LET will have different values for *E* and therefore different track-widths. The particle with lower *Z* will have a narrower track-width and more localized energy deposition, and, in many experiments, has been shown to have a higher biological effectiveness than a particle with higher Z. However, in tissue, the higher Z nuclei often has a larger range and can traverse more cell layers than a lower Z nuclei at the same LET. The biological effects of different types of particles are usually compared using the ratio of doses that lead to an identical effect. This ratio is called the relative biological effectiveness (RBE) factor. Human data for low

LET radiation such as γ-ray or X-ray exposures leading to increased cancer risk has been studied in the survivors of the atomic-bombs in Japan during World War II, medical patients exposed therapeutically to radiation, and nuclear reactor workers. However, there is no human data for high LET radiation such as cosmic rays to make risk estimates. Therefore, RBEs where the dose in the numerator is that of γ-rays and the dose in the denominator of a nuclear particle being studied, is often used to compare results from biological experiments with nuclei created at particle accelerators to results of epidemiological studies in humans exposed to γ-rays or X-rays. RBE's vary widely with the biological endpoint, cell or animal system, type of radiation and doses used in experiments.

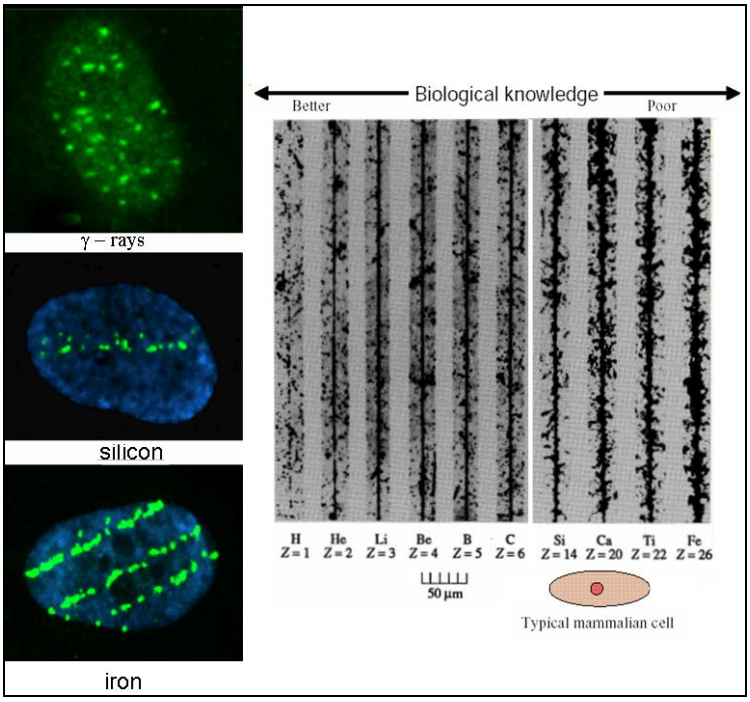

Figure 1. A comparison of particle tracks in nuclear emulsions and human cells. The right panel illustrates tracks of different ions, from protons to iron, in nuclear emulsions, clearly showing the increasing ionization density (LET=ΔE/Δx) along the track by increasing the charge Z. The left panel shows three nuclei of human fibroblasts exposed to γ-rays and Si- or Fe-ions, and immunostained for detection of γ-H2AX Each green focus corresponds to a DNA double-strand break (DSB). Whereas the H2AX foci in the cell that is exposed to sparsely ionizing γ-rays are uniformly distributed in the nucleus, the cells that are exposed to HZE particles present DNA damage along tracks (one Si- and three Fe-particles, respectively), and the spacing between DNA DSB is reduced at very high LET (Cucinotta and Durante, 2006).

Traditionally, it has been the role of advisory panels to make a subjective judgment of available RBE data to make estimates for human risk. Such judgment is used to define a radiation quality factor. For terrestrial radiation exposures quality factors, Q have been defined uniquely by LET, Q(LET). Values of Q from 1 to 30 have been used in the past for different LET values with Q=1 below 10 keV/μm and Q=30 at 100 keV/μm used at this time. However, for the more complex radiation environments in space, the inaccuracy of LET as a descriptor of biological effects has

been a long-standing concern. In the NASA 2010 model, radiation quality factors are redefined to have a dependence on two particle physical parameters, E and Z, rather than LET alone (Cucinotta *et al*., 2011). As particles penetrate through shielding materials or tissue and lose energy or undergo nuclear interactions, they produce secondary particles and then can have higher or lower quality factors than the primary particle. **Figure 2** illustrates this situation where the NASA radiation quality factor for solid cancer is plotted for different Z and E. Two examples that illustrate the complexity of the problem can be considered. First, if an Fe particle with energy above 800 MeV/u loses energy its Q-value will increase. Thus, shielding has made the situation worse. However, if the starting energy of Fe is below about 500 MeV/u, the shielding material can lower the cancer risk. A second example is for a fragmentation event of an Fe particle. When an Fe particle fragments, new particles of lower Z and E are produced that could be more biologically effective than the primary particle. Also, high energy neutrons, protons, and other light particles are produced in the same fragmentation event, thereby increasing the number of nuclear particles in the radiation field. For this reason, the understanding of the effectiveness of shielding materials and amounts is incomplete until the radiation quality factors and particle flux spectra are accurately defined.

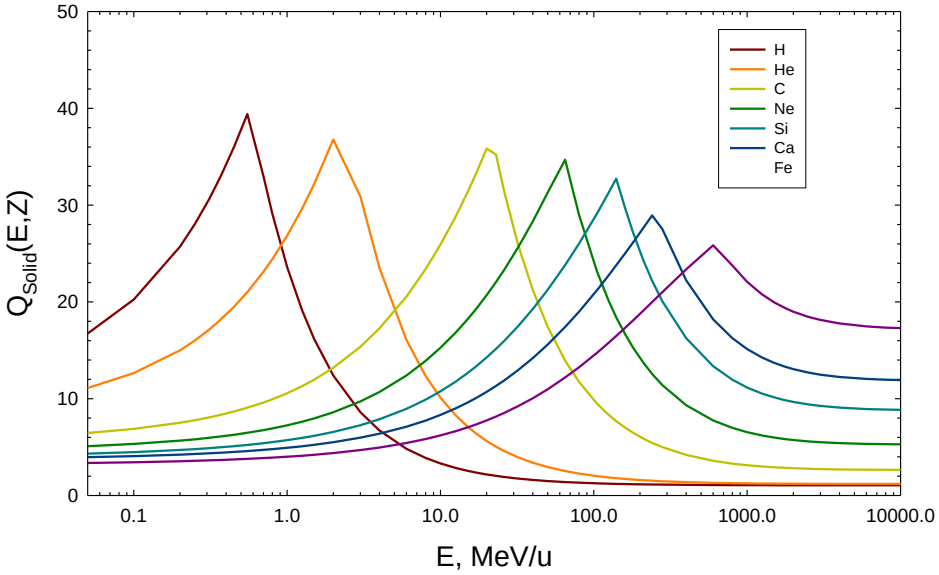

Figure 2. Dependence of the central estimates of the NASA radiation quality factor on particle kinetic energy for several GCR particles.

The multiplication of the absorbed dose by the quality factor is referred to as the dose equivalent, $H = Q(LET)\ D$, which has units denoted as 1 Sv (1 Sv = 100 rem; of 1 mSv = 0.1 rem). For calculating cancer risks, radiation transport codes are used to describe the atomic and nuclear collisions that occur inside spacecraft shielding and tissue, and resulting particle spectra averaged over the tissues of concern for cancer risk (e.g., lung, stomach, colon, bone marrow, etc.) to describe the organ dose equivalent, H_T. **Figure 3** shows a schematic of the nuclear reactions that occur where secondary radiation is produced both from the primary GCR and atomic constituents of spacecraft materials or tissue. **Figure 4** shows the resulting effects on the dose equivalent for solid cancer for increasing depth in different materials and at the transition

region into tissue. The advantages of liquid hydrogen are overestimated if the target fragments produced in tissue are not considered.

Because human epidemiological data are predominantly for high dose-rates, methods to estimate cancer risks at low dose-rates are needed. The traditional approach to this problem has been to estimate a dose and dose-rate reduction effectiveness factor (DDREF), which reduces the high dose-rate risk estimate for its application to low dose and dose-rates. DDREF values from 1.5 to 2.5 have been recommended in the past. The use of radiation quality factors and DDREFs is a major concern for space radiation risks because there are both quantitative and qualitative differences observed in experimental systems of cancer risks. It is not clear whether these quantities are sufficiently accurate to base risk estimates. NASA limits astronaut cancer risks to a lifetime REID of 3%. Because long space missions are projected to approach and exceed this risk limit, uncertainty analysis of the models and methods used to make risk estimates are performed including values and descriptions of H_T, Q, and DDREF, and the resulting impacts on the evaluation of shielding effectiveness. The importance of various GCR charge groups and energies in shielding material selection is dependent on the biological response model considered. Current radiobiological response models of cancer and other risks are not able to determine which shielding material is optimal under statistical tests that consider the uncertainties in such a calculation (Cucinotta *et al*., 2006). A more recent concern is the possibility of non-targeted effects or other peculiarities of the response of humans to radiation (Barcellos-Hoff *et al.*, 2007; Cucinotta and Chappell, 2010) that lead to a deviation from a linear response model. The value of radiation shielding and the importance of mission length could be diminished if biological responses are sublinear with increasing doses.

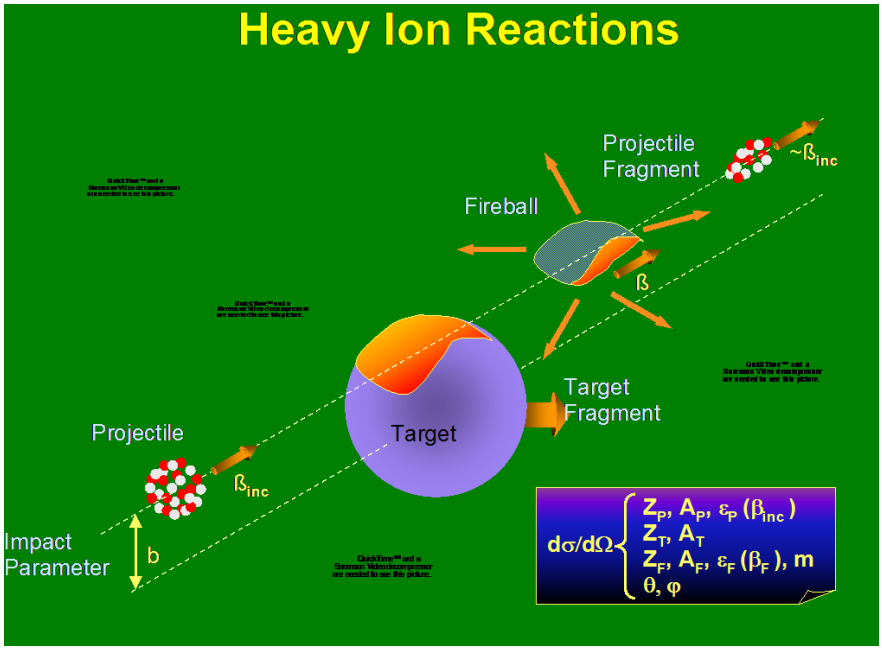

Figure 3. Schematic diagram of a relativistic heavy ion reaction showing the projectile and target fragments and fireball and their dependence on the impact parameter (from Walter Schimmerling).

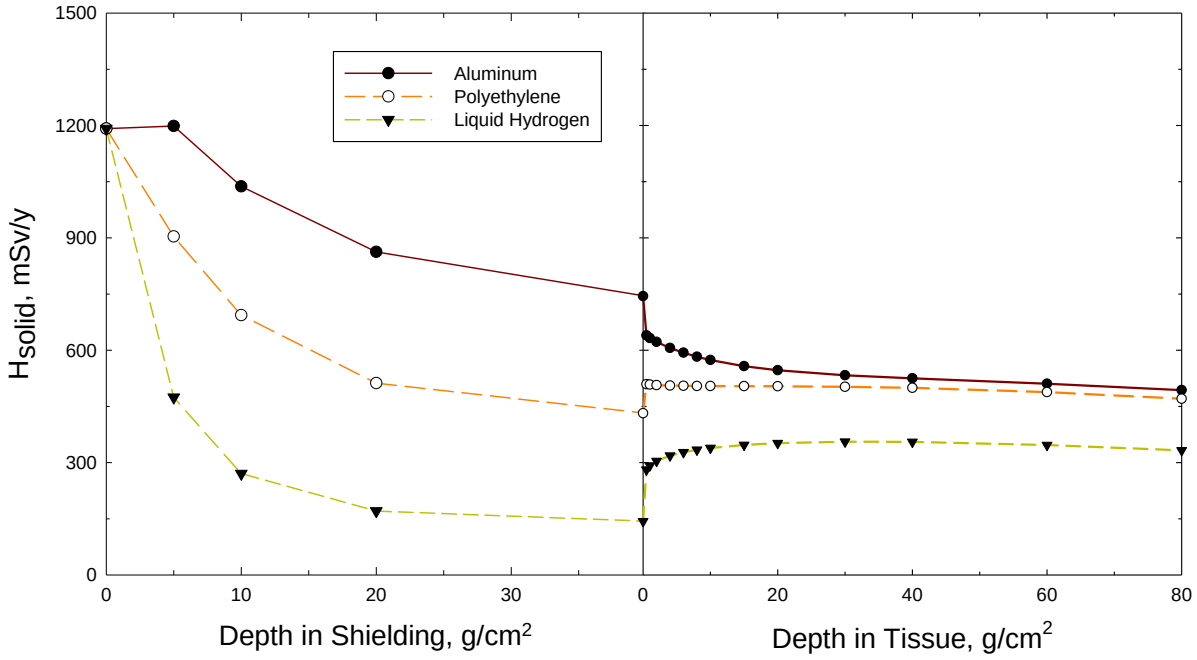

Figure 4. Transition effects at the shielding-tissue boundary on dose equivalents for tissue behind 40 g/cm^2 of aluminum, polyethylene or liquid hydrogen shielding. Transition effects increase as material atomic composition becomes more distinct from tissue due largely to target fragment production, which leads to low energy protons, helium and other light particles with large quality factors.

2.2 Shielding of Solar Particle Events

The key factor in SPE shielding is the energy distribution of protons and other possible solar particles such as He (Cucinotta *et al*., 1995). The 30 MeV proton fluence denoted as F_{30MeV}, is a useful measure since this is about the minimum energy proton that can penetrate thin shielding such as a space suit to reach internal organs. SPEs occur about 5 to 10 times per year, except near solar minimum, and consist largely of protons with kinetic energies from below 1 MeV up to a few hundred MeV. Kim *et al*. (2009) have ranked each event by the proton fluence above 30 MeV to form a probability distribution of the likelihood of an event of a given size for a specified mission length using hazard analysis (**Figure 5**). Of the nearly 400 SPE's observed in the space age (since 1955), only 41 have $F_{30MeV}>10^8$ per cm^2. The majority of SPEs with F_{30MeV} below this level lead to small doses (<0.01 Gy) in tissue. Furthermore, no events would have led to acute radiation death with minimal shielding due to their cumulative organ dose and dose-rates (Hu *et al.* 2009). Thus, only a small percentage (<5%) would lead to significant health risks if astronauts were not protected by shielding, and even a smaller percentage would lead to immediate harm. At this time, there is very little capability to predict the onset time and to determine whether a large or small SPE would occur until many hours after an SPE has commenced. Thus, mission disruption may occur for many SPEs although the health risks are small.

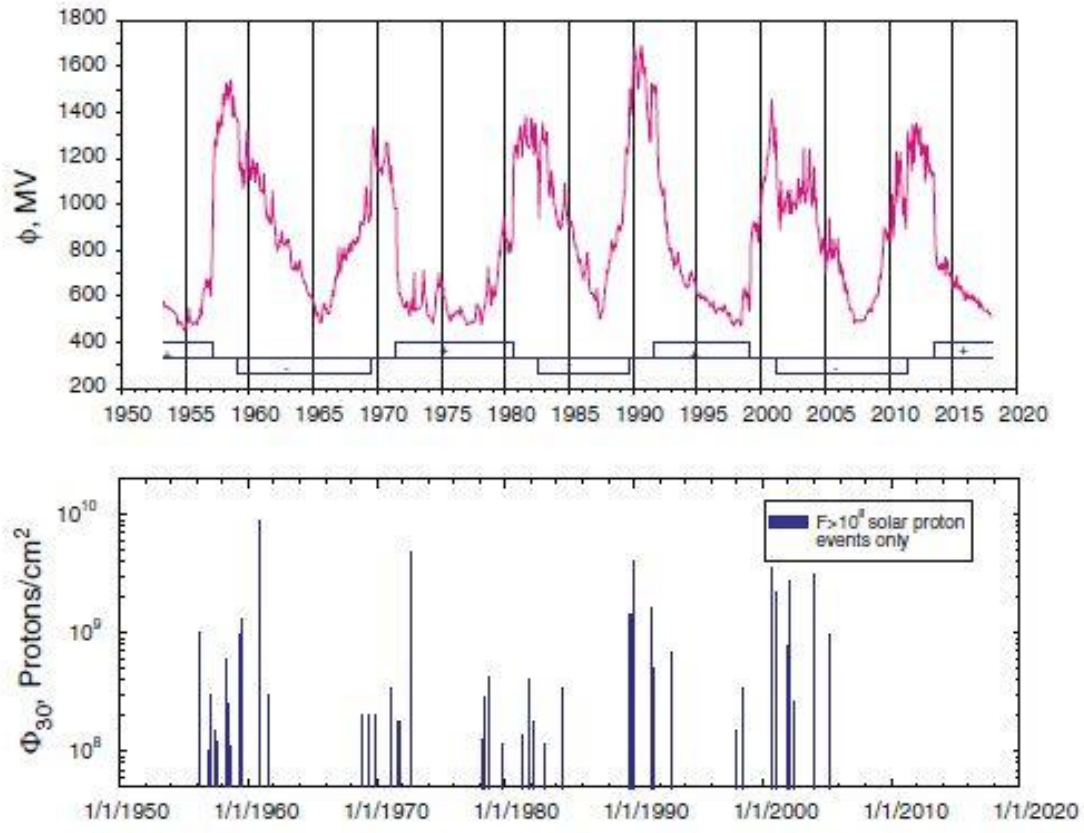

Figure 5. GCR deceleration potential (upper panel) and large SPEs (proton fluence $>10^8$ cm^{-2} at E>30 MeV) as a function of time (Kim *et al*., 2008).

The analysis of SPE organ doses shows that cancer and other late effects are the major concern for SPE exposure to astronauts with acute risks less of a concern (Hu *et al*., 2009). The results also show that the integral 30 MeV proton fluence is a weak predictor of organ doses, and more recent analysis shows the sufficient improvements when the 100 MeV integral proton fluence is used as a predictor (Kim *et al*., 2009). The situation would be different for extravehicular activities (EVAs) where doses can reach high levels for many events; however, space suit materials and design reduce exposures to some extent (Wilson *et al*., 2003). Optimizing mass through material selection and topological considerations are the focus for SPE shields. Shielding approaches must be developed for transit vehicles, planetary habitats, and EVAs including pressurized rovers, each of which has specific limitations (ASEB, 2008).

Because SPEs last only several hours at the peak exposure rates, localized shielding approaches including EVA shielding, portable shielding, and using crew sleep quarters as storm shelters are considered to be sufficient for SPE protection. Mass requirements on the order of 1000 kg are needed to provide a storm shelter protection for a crew of 3 when optimal material selection and topologies within vehicles or habitats are considered. For EVA shielding nearby pressurized rovers are advantageous, however spacesuit design and shielding blankets or coats made of hydrogenous materials to cover vital organs are advantageous.

2.3 Novel and In-situ Shielding Materials

The selection of materials can lead to significant reductions in the mass costs for SPE shielding, and is of interest in GCR radiation protection. Polyethylene has been identified as a useful structural polymer for spacecraft shielding with various fabrication strategies developed for damage-tolerant stiff structure and inflatable vehicles (Wilson, 1991). An important challenge is how to form high-density polyethylene fiber with polyethylene matrix and bond the resulting composite face sheets to form polyethylene foams. Approaches considered are plastic thermo-sets, aliphatic systems, and e-beam curing. Aliphatic systems lose strength at both low and high temperatures to be expected under space conditions. Wilson (Wilson *et al*. 2003) has discussed the usage of aliphatic/aromatic hybrid polymers as improvement to a purely aliphatic systems. Carbon nano-tubes with high hydrogen content offer a distinct approach and could be investigated for improved structural layouts.

Because of the high costs to launch mass, in-situ shielding on the lunar or Mars surface is of interest and may require distinct approaches since a higher relative fraction of astronaut exposures on the Mars surface are due to neutrons compared to the lunar surface due to the Mars atmosphere both depleting heavy ions and adding neutrons. The exposure to astronauts may depend on which region of Mars a habitat occupies (Wilson *et al*. 2001), because large variations in secondary neutrons can occur due to the soil composition as well as seasonal variations due to the presence of protective ice (water or perma-frost). Landing sites will likely be chosen by science requirements; however, they may require distinct shielding approaches dependent on the fractional contribution from neutrons to the total risk. Digging regolith to shield planetary habitats with bring-along equipment is one approach considered. However, the mass of the equipment needs to be considered. The moon is known to contain lava tubes as well as craters that partially shield radiation, and Mars has similar geographical features to increase habitat shielding. In-situ hydrogen or perhaps launched boron could be used to create regolith shielding bricks; however, this will require new manufacturing approaches on planetary surfaces.

2.4 Shielding Performance Tests

Aluminum structures have been the mainstay of spacecraft. Also, it is clear that hydrogen is certainly the optimal material for radiation protection. Materials with atomic constituents heavier than aluminum such as steel or lead produce too many neutrons to be of interest for space radiation protection. With these ideas in mind, Wilson (Wilson *et al.* 1995; 2001) devised a shielding performance index to bound material effectiveness relative to aluminum when considering different biological response models. Performance indexes from 2 to more than 10 are possible with typical amounts of spacecraft shielding, albeit the calculations used only a minimal amount of tissue shielding and thus overestimated shielding material performance. These results suggested that high hydrogen content materials could provide significant benefits compared to aluminum, especially if amounts > 30 g/cm^2 could be afforded in vehicle designs. However, it is unclear what the true performance of these materials would be because of the uncertainties in risk models for HZE particles, which were not considered by Wilson *et al.* (1996). A reduction in the point estimate of dose equivalent or risk could result from assigning

the incorrect biological effectiveness to different particles. It is for this reason that uncertainty analysis is necessary for GCR shielding evaluations. Cucinotta *et al.* (2006) developed a statistical test of shielding performance that considers the uncertainties in various factors that contribute to risk evaluation. For shielding evaluation, only uncertainties related to estimating the changes in changing radiation field and biological effectiveness represented by the radiation quality factor were considered. In this report, we use a similar approach, however using new definitions of radiation quality factors and uncertainty estimates for space physics and quality factors (Cucinotta *et al*., 2011).

3.0 Cancer Risk Projection Model

The instantaneous cancer incidence or mortality rates, λ_I and λ_M, respectively, are modeled as functions of dose D, or dose-rate D_r, gender, age at exposure a_E, and attained age a or latency L, which is the time after exposure $L=a-a_E$. The λ_I (or λ_M) is a sum over rates for each tissue that contributes to risk, λ_{IT} . These dependencies vary for each cancer type that could be increased by radiation exposure. The total REID is calculated by folding the instantaneous radiation cancer incidence rate with the probability of surviving to time t, which is given by the survival function $S_0(t)$ for the background population times the probability for radiation cancer death at previous time, and then integrating over the remainder of a lifetime (and summing over each tissue):

$$(1) \quad REID(a_E, D) = \int_{a_E} dt \lambda_M(a, a_E, D) S_0(t) e^{-\int_{a_E}^{t} dz \lambda_M(z, a_E, D)}$$

where z is the dummy integration variable. After adjustment for low dose and dose-rates through the DDREF and radiation quality, the tissue-specific, cancer incidence rate for an organ dose equivalent, H_T, can be written as a weighted average of the multiplicative and additive transfer models, often called a mixture model:

$$(2) \quad \lambda_{IT}(a_E, a, H_T) = [v_T ERR_T(a_E, a)\lambda_{0IT}(a) + (1 - v_T) EAR_T(a_E, a)] \frac{H_T}{DDREF}$$

where v_T is the tissue-specific transfer model weight, λ_{0IT} is the tissue-specific cancer incidence rate in the reference population, and where ERR_T and EAR_T are the tissue-specific excess relative risk (ERR) and excess additive risk (EAR) per Sievert, respectively. The hazard rates for cancer mortality λ_M are modeled with similar approaches following the BEIR VII report (2006). Tissue weights assumed in the NASA 2010 model are shown in **Table 1** along with recommendations from other reports. In the NASA 2010 Model (Cucinotta and Chappell 2011; Cucinotta *et al*., 2011), the United Nations Special Committee on the Effects of Atomic Radiation (UNSCEAR) report fitted EAR and ERR models are used for most tissue sites with the results from Preston *et al.* (2007) for a few tissues not reported by UNSCEAR. The ERR function fitted to the Life-Span Study (LSS) of the Japanese atomic-bomb survivors data was:

$$(3) \quad ERR(a, a_E, L, D) = (\alpha D + \beta D^2) e^{\gamma D} \exp[\kappa_1 1_S + \kappa_2 \ln(a - a_E) + \kappa_3 \ln(a) + \kappa_4 \ln(a_E)]$$

with a similar form for the EAR function. A linear dose response model provided the best fits to the tissue-specific cancer incidence data for solid cancers. For leukemias, the linear-quadratic model provided the best fit. The addition of the latency dependence, $L=a-a_E$, was significant for several tissues, including EAR models for colon, breast, and non-melanoma skin cancer, and ERR and EAR functions for the category of all other solid cancer incidence. For breast and thyroid cancers, the NASA 2010 models follows BEIR VII, which recommended the use of results from a meta-analysis of several exposed cohorts, replacing results from the LSS with additive transfer models used for breast cancer (Preston *et al*., 2002) and multiplicative transfer models used for thyroid cancer (Ron *et al*., 1995). For estimating cancer risks for low dose or dose-rate exposures, NCRP Report 132 (NCRP 2000) used a DDREF of 2. The BEIR VII Report recommended a DDREF of 1.5 based on Bayesian analysis of the LSS data and a select group of mouse tumor studies. The NIH uses (NIH 2003) a values close to 1.75, which is the choice for the NASA 2010 model (Cucinotta and Chappell, 2011).

Table 1. Tissue-specific Transfer Weight ν_T for Multiplicative Risk Transfer. Additive risk transfer weight is then given by $1-\nu_T$. Values described on page 126 of NCRP Report No. 132 (2000), and from pages 275-276 of BEIR VII (2006).

Tissue	*NCRP No. 132*	*BEIR VII*	*NASA 2010*
Lung	0.5	0.3	0.5
Breast	0.5	0**	0**
Thyroid	0.5	1.0**	1.0**
stomach, colon, liver, esophagus	0.5	0.7	0.7
Leukemia	0.0	0.7	0.5
All Others	0.5	0.7	0.5

***Based on meta-analysis results described in BEIR VII.*

3.1 Adjusting U.S. Cancer Rates for Never-Smokers Cancer Estimates

Cancer rates for gender-specific never-smokers (NS) are used to represent a reference population and age-specific rates for lung cancer and relative risk factors derived from literature searches for other cancers. Age and gender-specific NS lung cancer rates were recently compiled by Thun *et al.* (2009) from an analysis of 13 cohorts and 22 cancer registries. These rates are used for our analysis of radiation lung cancer risks for NS. For other cancers, we use Centers for Disease Control and Prevention (CDC) estimates of proportions of cancer deaths for smokers (S) and former smokers (FS) in the U.S. population. CDC estimates (2010) of relative risks (RR) between these populations were used for cancers of the esophagus, stomach, bladder, and oral cavity, and for acute myeloid leukemia. Other published sources are used for several tissue sites, which are liver, colorectal, and lymphomas (Liang *et al*., 2009; Sandler *et al*., 2003; IARC 1986). The fraction of cancers categorized in the "remainder" category are estimated based on the number of cases reported by Preston *et al*. (2007) for different cancer types related to smoking including pharynx, larynx, and pancreas. Cancer rates reported for the U.S. population are made up of populations of S, FS, and NS with proportions f_S, f_{FS}, and f_{NS}, which leads to:

$$(4) \quad \lambda_{0T}(a) = f_S \lambda_{0T}^{S}(a) + f_{FS} \lambda_{0T}^{FS}(a) + f_{NS} \lambda_{0T}^{NS}(a)$$

The RR of S and FS compared to NS, RR_S and RR_{FS}, respectively are then used to compare rates for NS to the U.S. average rates,

$$(5) \quad \lambda_{0T}^{NS}(a) = \frac{\lambda_{0T}(a)}{(RR_S f_S + RR_{FS} f_{FS} + f_{NS})}$$

We used the 2005 U.S. population data from surveillance, epidemiology, and end results (SEER) (2006) and the CDC (2008) to represent the average U.S. population, and CDC estimates of fractions of populations for S, FS, and NS for males and females above age 40 y. The resulting estimates of RR for NS compared to the U.S. population are shown in **Table 2**. For NS risk estimates, we considered their longer lifespan due to their reduced mortality for cancer, or for circulatory and pulmonary diseases. Age-specific rates for all causes of death for NS were not available and, instead, we considered the survival probability for the average U.S. population and made adjustments for the age- and gender-specific rates for these diseases (CDC 2008; Malarcher *et al.*, 2000). Here we modified the survival probability in Eq. (1) to adjust for lower rates for cancers and for circulatory and pulmonary diseases that are also linked to tobacco use (CDC 2008).

Table 2. Estimates of RR for NS Compared to Average U.S. Population for Several Cancers Related to both Smoking and Radiation Exposure

	RR to NS			
Males	**Current smokers**	**Former smokers**	**Never-smokers**	**RR(NS/US)**
Esophagus	6.76	4.46	1	0.27
Stomach	1.96	1.47	1	0.71
Bladder	3.27	2.09	1	0.50
Oral Cavity	10.89	3.4	1	0.23
Liver	2.25	1.75	1	0.63
Colorectal	1.19	1.21	1	0.89
Leukemia	2	1.5	1	0.69
Remainder	4	2.5	1	0.43
Lung*	23.26	8.7	1	0.11
Females	**Current smokers**	**Former smokers**	**Never-smokers**	**RR(NS/US)**
Esophagus	7.75	2.79	1	0.35
Stomach	1.36	1.32	1	0.85
Bladder	2.22	1.89	1	0.65
Oral Cavity	5.08	2.29	1	0.46
Liver	2.25	1.75	1	0.67
Colorectal	1.28	1.23	1	0.88
Leukemia	2	1.5	1	0.74
Remainder	4	2.5	1	0.48
Lung*	12.69	4.53	1	0.23

**Lung data shown only for comparison, where risk calculations made using Age-specific rates described in the text. For males, current smokers, former smokers, and never-smokers are estimated at 24, 40, and 36% of the population above age 50 y. For females we use 18, 35, and 47% for these percentages (CDC-MMWR, 2010).*

3.2 Space Radiation and Organ Exposures

For calculations of space radiation tissue-specific cancer risks, Eq. (2) is used for the cancer incidence risk rate with the organ dose equivalent estimated using the HZETRN Code (Wilson *et al.*, 1994) with quantum multiple scattering fragmentation (QMSFRG) model cross sections and Badhwar-O'Neill GCR environment (Cucinotta *et al*., 2011). For GCR the use of risk assessment quantities based on absorbed dose is expected to have shortcomings and instead the NASA 2010 derived radiation quality descriptors of biological effectiveness based on particle track structure and fluence that were then expressed as radiation quality factors (Cucinotta *et al*., 2011). Here, a cancer risk cross section representing the probability per particle is written as:

$$(8) \quad \Sigma(Z,E) \;=\; \Sigma_0[P(Z,E)+\frac{\alpha_\gamma}{\Sigma_0}(1-P(Z,E))L]$$

with

$$(9) \quad P(Z,E) \quad = \quad \left(1-e^{-Z^{*2}/\kappa\beta^2}\right)^m$$

where the three parameters of the model (Σ_0/α_γ, m, and κ) based on subjective estimates of results from radiobiology experiments. A radiation quality factor function is then found as:

$$(10) \quad Q_{NASA} \quad = \quad (1-P(E,Z))+\frac{6.24(\Sigma_0/\alpha_\gamma)P(E,Z)}{LET}$$

The NASA quality factor depends on both particle charge number, Z, and kinetic energy, E, and not linear energy transfer, LET, alone as assumed in the International Commission on Radiological Protection (ICRP) definition of quality factors (ICRP 1990; ICRP 2003; NCRP 2000). Distinct quality factors for estimating solid cancer and leukemia risk are used, Q_{solid} and $Q_{leukemia}$, respectively. The parameters that enter Eq. (8) to Eq. (10) have straightforward biophysical interpretations: Σ_0 is the maximum value of the cross section, which is related to RBE_{max} for the most biologically effective particle types. *m* is the slope of the cross section for increasing ionization density. κ determines the saturation value of the cross section, where the RBE begins to decline due to "overkill" effects. α_γ is related to the initial slope of the gamma-ray dose response. Only the ratio Σ_0/α_γ enters into model calculations, and not the individual values of these parameter. For solid cancer risks, radiobiology data are sparse. However, the largest RBE for HZE nuclei is in the range from 20 to 50 for solid tumors in rodents, and for chromosomal aberrations and mutations in human cells. A lower value is observed for leukemia (Weil *et al*., 2009). This assumes a linear dose response at low particle dose, ignoring non-targeted effects (NTEs) or other possible mechanisms that would lead to deviation from linearity at low fluence. Calculations with the NASA 2010 model include uncertainty analysis through the use of probability distribution functions (PDFs) to represent subjective assessments of ranges for each of the parameters with median values shown in **Table 3**. We also assume a description of "thindown" at low energies, where the track width of a particle becomes smaller than the biological target. Here, at low energies, the risk cross section is modified by the factor, $P_E=1-\exp(-E/E_{TD})$ to account for thindown. The value of $E_{TD}=0.2$ is based on experimental data for H and He. This factor has a very small impact for heavy ions since at low E they make a very small contribution to GCR or SPE exposures. The parameter κ is assumed to have distinct values for light and heavy ions (**Table 3).** The cancer risk cross section or related quality factor is expressed in terms of the track structure parameter, $X_{tr}= Z^{*2}/\beta^2$, using the Barkas form for the effective charge function. The quality factor has an additional dependence on LET, which relates the particle track structure to the absorbed dose (Cucinotta *et al*., 2011). The preferred slope on the rising side with increasing ionization density of m=3 is different than the ICRP Q(LET), which rises approximately as m=2.

Table 3. Cancer Risk Cross Section or Quality Factor Parameters for Solid Cancer and Leukemia Risks*

Parameter	Solid Cancer	Leukemia
m	3	3
κ	550 (1000)	550 (1000)
Σ_0/α_γ, μm^2 Gy	7000/6.24	1750/6.24
E_{TD}	0.2 MeV/u	0.2 MeV/u

**Values in parentheses for when distinct values for light ions ($Z \leq 4$) are to be used.*

For calculations for a specific particle described by *Z* and *E*, Eq. (2) is replaced by

$$(11) \quad \lambda_{ZI}(F_T, a_E, a) = \lambda_{\gamma I}(a_E, a)\left\{D_T(E,Z)(1-P(Z,E)) + (\Sigma_0/\alpha_\gamma)P(Z,E)F_T(Z,E)\right\}$$

where $\lambda_{\gamma I}$ is the inner bracketed terms in Eq. (2) that contains the ERR and EAR functions for individual tissues. Using the HZETRN code or similar radiation transport codes, the fluence spectra, $F(X_{tr})$ can be found by transforming the energy spectra, $\phi_j(E)$ for each particle, *j* of mass number and charge number, A_j and Z_j respectively as:

$$(12) \quad F(X_{tr}) = \sum_j \left(\frac{\partial X_{tr}}{\partial E}\right)^{-1} \phi_j(E)$$

where we evaluate the Jacobian in Eq. (12) using the Barkas (1963) form for the effective charge number given by

$$(13) \quad Z^* = Z(1-e^{-125\beta/Z^{2/3}})$$

The tissue-specific cancer incidence rate for GCR or SPEs can then be written:

$$(14) \quad \lambda_{IT} \approx \lambda_{I\gamma}\left\{\sum_j \int dE\phi_{jT}(E)S_j(E)(1-P(X_{tr})) + (\Sigma_0/\alpha_\gamma)\int dX_{tr}F(X_{tr})P(X_{tr})\right\}$$

The first term on the right-hand side of Eq. (14) can be well approximated by the tissue averaged absorbed dose times the low LET risk coefficient. This approximation can be shown to lead to <10% overestimation of its true value. However, in REID calculations, the error is even smaller because the second term of the right-hand side of Eq. (14) is dominant. We modified the HZETRN and baryon transport computer code (BRYNTRN) codes to perform the exact calculation; however, for the Monte-Carlo uncertainty analysis described below, we use the following form for the radiation cancer rate for the mixed particle and energy fields in space:

$$(14') \quad \lambda_{IT} \approx \lambda_{I\gamma}\left\{Dose + \Sigma_0\left[\int dX_{tr}F_{LI}(X_{tr})P_{LI}(X_{tr}) + \int dX_{tr}F_{HI}(X_{tr})P_{HI}(X_{tr})\right]\right\}$$

where we distinguish spectra for light ions (Z≤4), F_{LI} from heavy ions, F_{HI} (Z>4). A summation over all cancer types is made for the radiation contribution to the survivor function in evaluating tissue-specific risks, and a further summation over all cancer types to evaluate the overall cancer risk.

In organ exposure evaluations, fluence spectra are averaged over each tissue using body shielding models. In **Figure 6**, we show the differential risk of exposure-induced cancer incidence (REIC) spectra versus X_{tr} at solar minimum for 20 g/cm^2 aluminum shielding for a Mars and an International Space Station (ISS) mission. Calculations are made with the HZETRN code using the Badhwar and O'Neill GCR model (1992) and QMSFRG nuclear cross section database (Cucinotta *et al.,* 2007). Results are shown on a linear-log plot such that the area under the curve for each decade of X_{tr} is equally weighted. Leukemia risk shows a reduced maximum Q-value compared to solid cancer risks, resulting in particles at lower values of X_{tr} making larger contributions compared to solid cancer risks. **Figure 6** shows sharp spikes at increasing values of Z^2 for each GCR charge group. For example, at small values of X_{tr}, we see peaks at 1 and 4, corresponding to protons and He nuclei. At large values of X_{tr}, we observe a prominent peak near Z^{*2}/β^2 = 676 corresponding to relativistic Fe nuclei. These sharp peaks correspond to the contributions from relativistic particles, with broader peaks for deep-space exposure due to contribution of low- to medium-energy GCR not present in the ISS orbit due to the Earth's geomagnetic field.

In **Figure 7,** we compare calculations of annual Effective dose for several shielding materials in the ICRP model (**Figure 7a**) to the NASA recommended model (**Figure 7b**) for deep-space missions at solar minimum. The ICRP model provides higher estimates at shallow shielding depth due largely to its higher estimation of contributions for relativistic particles than the NASA model. At deep shielding depths, the NASA model gives higher estimates due to its assignment of higher biological effectiveness to low-energy proton and helium nuclei produced by neutrons and other particles and from atomic slowing-down of primaries. For the various mission and shielding scenarios, differences in Effective doses are on the order of 10 to 30%; however, the NASA model allows for an improved uncertainty assessment to be made than the ICRP Q function whose parameters are difficult to relate to biophysical interpretation. Of note is that shielding only provides a minor reduction in GCR organ dose equivalent. Most of the reduction occurs in the first 20 g/cm^2 of material at solar minimum. The reduced number of low-energy particles at solar maximum reduces even this benefit from shielding. To significantly reduce GCR beyond this initial reduction would require several meters of hydrocarbon shielding.

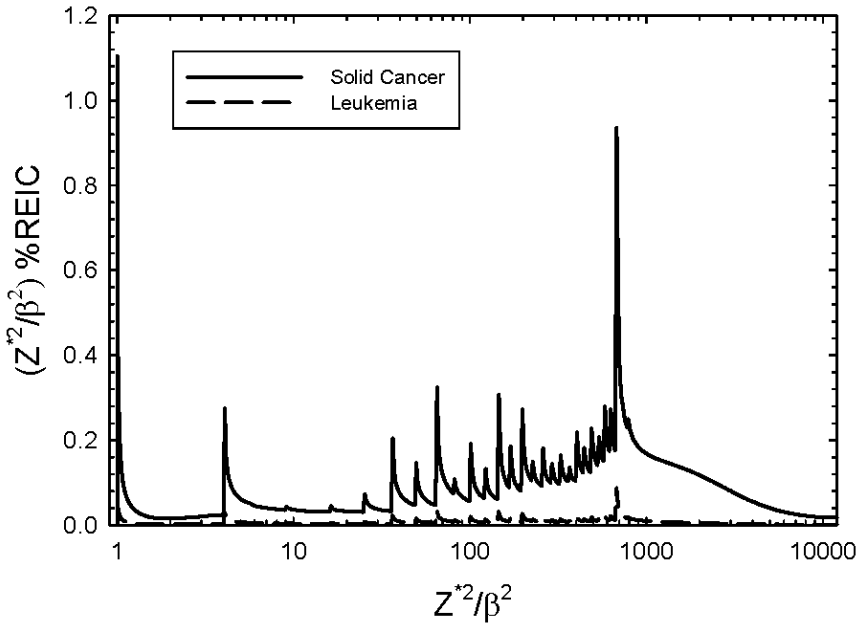

Figure 6a. Leukemia and solid cancer risk distribution for 40-y females versus Z^{*2}/β^2 on 6-month ISS mission at solar minimum with 20 g/cm^2 of aluminum shielding .

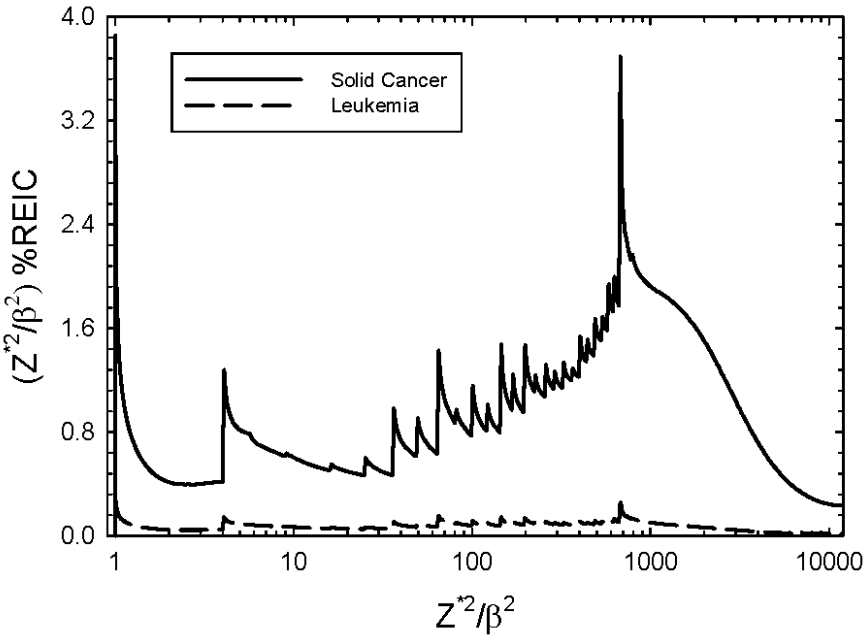

Figure 6b. Leukemia and solid cancer risk distribution for 40-y Females versus Z^{*2}/β^2 for 30-month Mars mission including 18-month surface stay at solar minimum with 20 g/cm^2 of aluminum shielding.

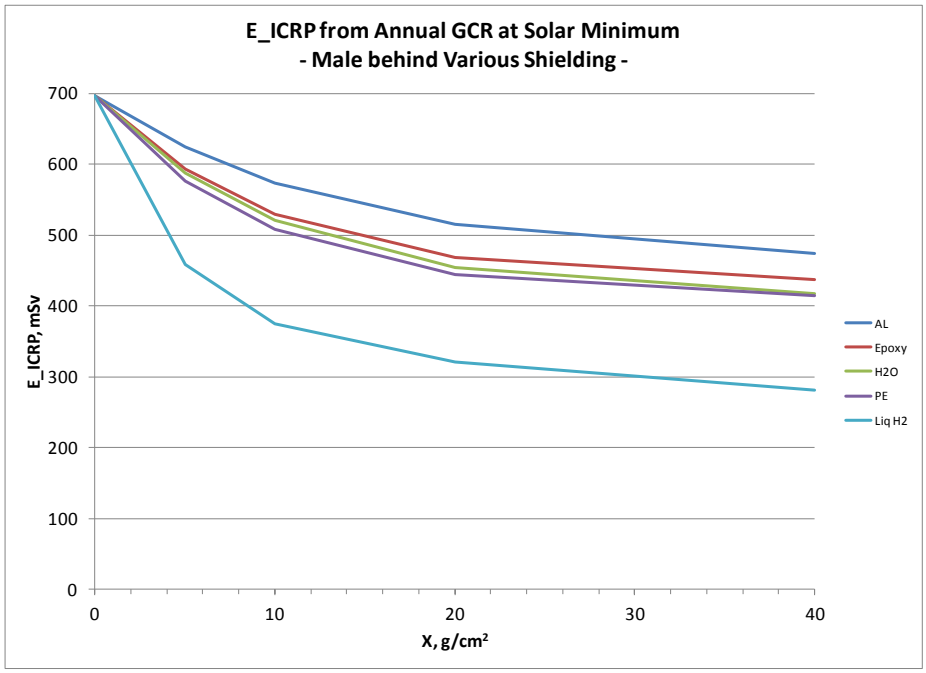

Figure 7a. Comparisons on depth-Effective dose estimates versus shielding thickness using the ICRP definition of quality factors for several materials. Calculations are for 1-year GCR exposures at solar minimum.

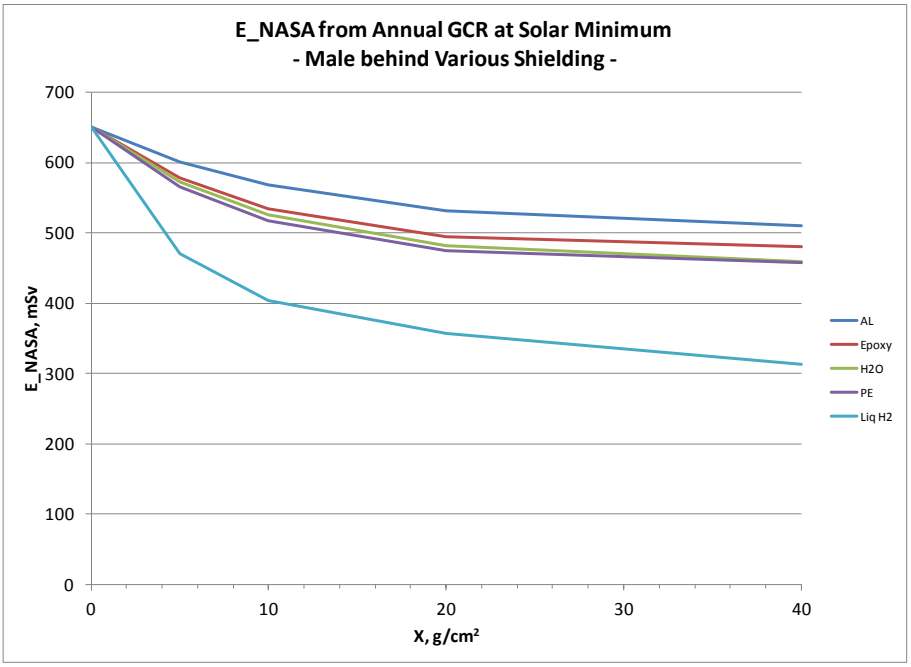

Figure 7b. Comparisons on depth-Effective dose estimates versus shielding thickness using the NASA Solid cancer definition of quality factors for several materials. Calculations are for 1-year GCR exposures at solar minimum.

3.3 Uncertainty Analysis

To propagate uncertainties across multiple contributors, we performed Monte-Carlo simulations sampling over subjective PDFs that represent current knowledge of factors that enter into risk models (NCRP, 1997; 2006; Cucinotta *et al.,* 2001*,* 2006; 2011). In a simplified manner, we can write a risk equation as a product of several factors including the dose, *D*, quality factor, *Q*, a low LET risk coefficient normally derived from the data of the atomic-bomb survivors, R_0, and the dose and dose-rate reduction effectiveness factor, *DDREF*, that corrects risk data for dose-rate modifiers. Monte-Carlo uncertainty analysis uses the risk equation, but are modified by normal deviates that represent subjective weights and ranges of values for various factors that enter into a risk calculation. First, we define $X \in R(x)$ as a random variate that takes on quantiles $x_1, x_2, \ldots, x_n$ such that $p(x_i) = P(X=x_i)$ with the normalization condition $\Sigma\, p(x_i)=1$. $C(x_i)$ is defined as the cumulative distribution function, $C(x)$, which maps X into the uniform distribution $U(0,1)$ and we define the inverse cumulative distribution function $C(x)^{-1}$ to perform the inverse mapping of $U(0,1)$ into x: $x=C(x)^{-1}$. Then we write for a simplified form of the risk equation for a Monte-Carlo trial, ξ:

$$(15) \quad Risk_{\xi} = R_0(age, gender)\frac{FLQ}{DDREF}\left\{\frac{x_{R_0}x_{phys}x_Q}{x_{D_R}}\right\}_{\xi}$$

where R_0 is the low LET risk coefficient per unit dose, the absorbed dose, D, is written as the product of the particle fluence, F and LET, L, and Q the radiation quality factor. The x_{R0}, x_{phys}, x_{Dr}, *and* x_Q are quantiles that represent the uncertainties in the low LET risk coefficient, the space physics models of organ exposures, dose-rate effects, and radiation quality effects, respectively. Monte-Carlo trials are repeated many times, and resulting values binned to form an overall PDF taken into account each of the model uncertainties. In practice, the risk model does not use the simple form of Eq. (15). Instead, risk calculations are made using the REIC described by Eq. (1).

PDF functions describing the uncertainties to the quantiles, x_{ξ} for the various parameters in the model are described in **Table 4** from the recent report by Cucinotta *et al*. (2011). Two modifications are to introduce tissue-specific statistical uncertainties and to include uncertainties in the estimate of RR for NS compared to the U.S. average. The subjective PDFs are then employed in the Monte-Carlo calculation to describe a given space radiation scenario as described previously (Cucinotta *et al.,* 2001; 2006; 2011). The point estimate for Q_{max} of 40, occurs for the most effective proton energy (~ 0.5 MeV). Values assigned give more weight to the animal model solid tumor data and are influenced by fractionation studies that suggest that higher RBEs are possible. The resulting PDF has a 95% C.I. for the maximum value of Q for solid cancer as [14, 70], which covers most of the range of values from Fe nuclei tumor induction and earlier neutron studies reflective of low energy protons. In **Table 4**, we use a GM=0.9 for the PDF associated with Σ_0 / α_γ with the expectation that some tissues would have lower values as found for leukemia; however, there is a lack of information to make a more informed choice. In an alternative model of the radiation quality uncertainties, we assume that the slope, m, is correlated with the position of the maximum value of Q as determined by the

value of κ. After studying the functional dependence of the parameters of Eq. (10), we find the position of the maximum Q is held fixed for differential values of *m* if we use the constraint:

$$\kappa(m) = \frac{4\kappa_0}{(m+1)} \quad (16)$$

where κ_0 is the estimated value from **Table 3**. This alternative uncertainty assessment assumes that the kinetic energy for each Z at the maximum of the risk cross section for cancer induction in humans is fairly well described by the existing data. In this approach, uncertainties in the maximum Q value, slope of Q with changing X_{tr}, and kinetic energy at the Q maximum are described; however, these values are more constrained compared to the uncertainty analysis without this constraint. The alternative uncertainty model was applied using conditional Monte-Carlo sampling, where a random value of *m* is selected from its PDF prior to sampling for the κ value with central estimate defined by Eq. (16).

Table 4. Summary of PDF for Uncertainty Components in NASA Model

Uncertainty Contribution	PDF form for Quantile, x_j	Comment
Low LET Model:		
Statistical Errors	See Cucinotta et al. (2012)	Tissue-specific values used
Statistical Errors in RR for NS	Normal (M=1.0; SD=0.25)	Applied to tissues considered in Table 3 for NS
Bias in Incidence data	Normal (M=1.0; SD = 0.05)	Based on NCRP Report 126
Dosimetry Errors	Log-Normal (GM=0.9, geometric standard deviation [GSD]=1.3)	Based on Preston *et al*. (2007); UNSCEAR (2008)
Transfer model weights	Uniform distribution about preferred weight	Ignored for breast and thyroid cancers
DDREF	Log-Normal (GM=1.0; GSD=1.4)	DDREF=1.75; Truncated at 0.75 for inverse dose-rate probability <0.05
Risk Cross Section or Q:		
Σ_0/α_γ	Log-normal (GM=0.9; GSD=1.4)	GM<1 assumes existing data are biased to higher values
κ	Normal (M=1, SD=0.2)	Position of peak estimates suggests variation on sensitivity, target size/distributed targets
m	Discrete m=[1.5,2,2.5,3.,3.5,4] with weights [.05,.1,.2,.4,.2.,.05]	Values restricted over (1.5,4)
Physics Uncertainties:		
$F(Z^{*2}/\beta^2)$ for Z<5	Normal (M=1.05; SD=1/3)	HZETRN does not account for mesons, e- and γ-rays that are low charge and high velocity; may underestimate neutron recoils of low charge
$F(Z^{*2}/\beta^2)$ for Z≥5	Normal (M=1.0; SD=1/4)	HZETRN accurate at high Z

For estimating the statistical uncertainties for overall cancer risks from radiation, we previously used (Cucinotta *et al*., 2011) the recommendations from NCRP Report 126 (1997) for the statistical uncertainty in the total cancer risk derived from cancer mortality data of the LSS survivors. However, larger statistical uncertainties occur for tissue-specific risk estimates derived from cancer incidence data. The various reports on tissue-specific estimates of cancer risks (BEIR VII, 2006; UNSCEAR 2008; Preston *et al*., 2007) typically combine statistical uncertainties with dosimetry or other uncertainties in reporting confidence levels (CLs). The UNSCEAR report did not report uncertainty ranges for their model EAR and ERR functions, which further complicates assessments of tissue-specific statistical uncertainties. Methods to consider tissue-specific statistical uncertainties were considered in our recent report Cucinotta et al. (2012).

3.4 Shielding Performance Tests

The overall PDF found after propagating the various model uncertainties allows us to make a statistical test of the effectiveness of one material to another. We use the two-sample Kolmogorov-Smirnov (KS) statistical test (Elandt-Johnson and Johnson, 1999) as a non-parametric method to evaluate shielding performance of a test material compared to aluminum shielding. In the two-sample KS test, the cumulative probability (CDF) distribution of the REID in a baseline shielding configuration, $C_1(REID)$ and in a second material or configuration, $C_2(REID)$ are formed, and the maximum difference between the distributions in the positive direction (one-sided test) are considered for the case of an expected reduction in REID for the second material. The negative statistic corresponding to a REID decrease in a proposed shielding configuration compared to the baseline is given by:

$$(17) \quad Z^{-} = \max\left[C_1(REID) - C_2(REID)\right]$$

In the large sample limit, the condition for rejecting the null hypothesis at the significance level α and $y_{1-2\alpha}$, is found from the value of y for which the right-hand side of the following distribution, *Pr,* given in Eq. (18) is equal to α:

$$(18) \quad \lim_{N\to\infty} \Pr\{\sqrt{N} Z_{-} > y\} = 2\sum_{j=1}^{\infty} (-1)^{j+1} \exp(-2 j^2 y^2)$$

The distribution in Eq. (18) can be interpreted as a continuous-time stochastic process whose probability distribution is the conditional probability represented by Brownian motion.

4.0 Results and Discussion

In the following results, all transport calculations are made using the HZETRN code with QMSFRG nuclear interaction cross sections for heavy ions and light particles, except for solar protons events where transport calculations are made using the BRYNTRN code. The Badhwar-O'Neill GCR environment model (1992) is used for the transport code boundary condition. The computerized anatomical man model (CAMERA) is used to represent self-shielding of the different organs contributing to cancer risk (Billings *et al*., 1973). For calculations near solar maximum, we assume that an event identical to the August 1972 SPE occurred during the mission, which raised cancer risks beyond that of the GCR alone. The various uncertainties considered in the NASA 2010 model summarized in **Table 4** include those that are dependent on radiation type (space physics and radiation quality), and uncertainties that are independent of radiation quality (epidemiology data, DDREF, etc). For the shielding performance test, we will ignore the uncertainties that are not dependent on radiation type. Comparisons of REID and 95% CI for 20 g/cm^2 of aluminum or polyethylene shielding are shown in **Table 5** for the cases of all uncertainties, and radiation type dependent alone. Comparisons with either the uncorrelated or correlated Q-uncertainties as described in Eq. (16) are shown. **Figure 8** illustrates the differential (PDF) and cumulative distribution (CDF) of REID, comparing aluminum to polyethylene shielding of 20 g/cm^2. The PDF is well described as a log-normal distribution with significant skewness, making a statistical test based on normal distribution inappropriate. Therefore, a non-parametric test such as the KS test is needed for evaluating shielding performance to reduce cancer risk. **Tables 6 and 7** show detailed comparisons of %REID, and 95% CI for 1-year missions at solar minimum or solar maximum for different material types and thicknesses. The one-sided KS test is used to compare different materials relative to aluminum for potential risk reduction. For all cases, liquid hydrogen provides the best performance followed by polyethylene and water shielding. Epoxy shielding is only modestly different from aluminum for both REID reduction and for the significance of the reduction. We have not considered backward scattered particles in these comparisons. We expect the results for alternative materials to be modestly improved by their inclusion, since forward scattered particles dominate REID due to their larger quality factors, and aluminum would contain a larger number of backward scattered neutrons and other light particles compared to these other materials.

Aluminum shielding has been used in all human-rated spacecraft, to date. An alternative approach to replacing aluminum as the main spacecraft structural material could consider an aluminum structure with all internal equipments and localized shielding comprised of well-designed radiation shielding materials. **Tables 8 and 9** show results for a two layup configuration with the outer layer of 10 g/cm^2 aluminum configuration in all cases. The improvement for others materials is reduced with aluminum as the outer layer; however, statistically significant results are found at the larger shielding depths in most cases.

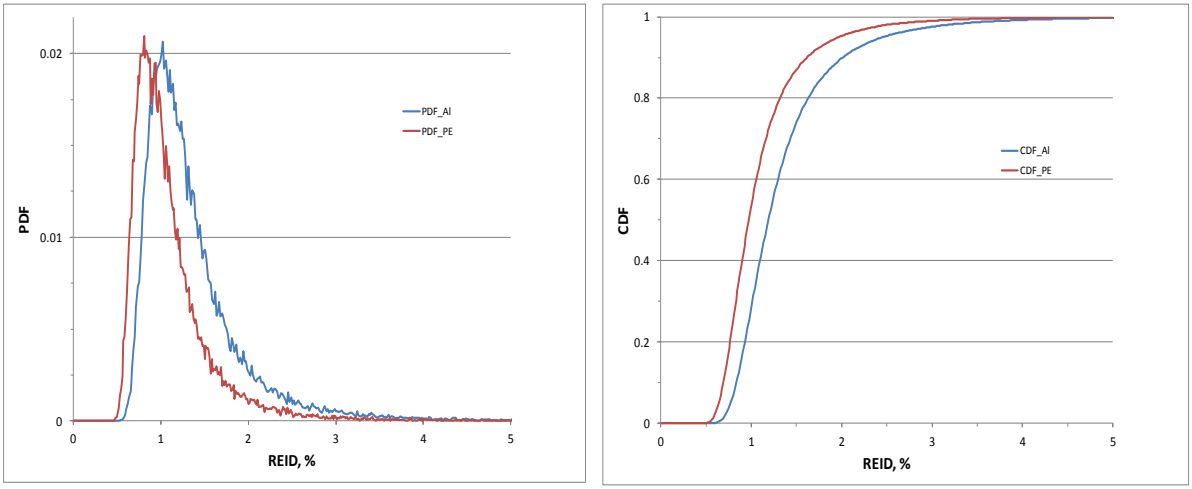

Figure 8. Comparison of PDF and CDF for US average males behind 20 g/cm^2 of aluminum or polyethylene shielding for 1-year missions in deep space at solar maximum with 1972 SPE.

5.0 Conclusions

In this paper, we considered the most recent NASA model of space radiation cancer risks and uncertainties, including new track structure based radiation quality factor functions to evaluate the effectiveness of different material types and amounts for reducing risks near solar minimum and solar maximum. There is continued interest in evaluating possible improvements in radiation shielding approaches compared to aluminum shielding. Because the probability distribution function for fatal cancer risk is highly skewed to large values of REID, we considered the non-parametric KS test to compare a test material to aluminum. Results show that only modest reductions in REID are found with increasing shielding amounts beyond a nominal shield of about 10 g/cm^2. However, the recent improvements in the NASA cancer risk projection model show that statistically significant improvements over aluminum shielding can be demonstrated at both solar maximum and solar minimum for shields of about 10 g/cm^2 or more for several materials. These results demonstrate the important value to NASA of radiobiology research, which is the principle mechanism to reduce uncertainties. Liquid hydrogen remains the optimal shielding material, but its performance can be overestimated if secondary radiation produced in tissue or the vessel containing the hydrogen are not considered. Nevertheless, developing new multifunctional shielding materials with higher hydrogen content compared to polyethylene is advocated.

Table 5. Comparison of %REID and 95% CLs for Aluminum and Polyethylene Shielding for all Uncertainties and Uncertainties Dependent on Radiation Type Alone

Annual GCR at Solar Minimum, Avg U.S. population							
Material	E (Sv)	All Uncertainty		Q-Uncorrelated		Q-Correlated	
		REID[95% CI], %	p-value	REID[95% CI], %	p-value	REID[95% CI], %	p-value
20 g/cm^2 Al	0.53	2.10 [0.70, 7.31]	3.10E-02	2.10 [1.22, 7.28]	1.03E-04	2.10 [1.27, 5.08]	4.81E-06
20 g/cm^2 PE	0.47	1.87 [0.62, 6.51]		1.87 [1.13, 6.61]		1.87 [1.18, 4.47]	
Annual GCR at Solar Minimum, NS							
Material	E (Sv)	All Uncertainty		Q-Uncorrelated		Q-Correlated	
		REID[95% CI], %	p-value	REID[95% CI], %	p-value	REID[95% CI], %	p-value
20 g/cm^2 Al	0.53	1.63 [0.54, 5.65]	2.67E-02	1.63 [0.94, 5.70]	7.32E-05	1.63 [0.99, 3.97]	3.85E-06
20 g/cm^2 PE	0.47	1.45 [0.50, 5.07]		1.45 [0.88, 5.14]		1.45 [0.92, 3.49]	
August 1972 SPE+Annual GCR at Solar Maximum, Avg U.S. population							
Material	E (Sv)	All Uncertainty		Q-Uncorrelated		Q-Correlated	
		REID[95% CI], %	p-value	REID[95% CI], %	p-value	REID[95% CI], %	p-value
20 g/cm^2 Al	0.3	1.18 [0.38, 4.23]	1.20E-05	1.18 [0.68, 4.28]	3.00E-12	1.18 [0.72, 2.97]	2.44E-16
20 g/cm^2 PE	0.24	0.96 [0.32, 3.42]		0.96 [0.57, 3.48]		0.96 [0.60, 2.36]	
August 1972 SPE+Annual GCR at Solar Maximum, NS							
Material	E (Sv)	All Uncertainty		Q-Uncorrelated		Q-Correlated	
		REID[95% CI], %	p-value	REID[95% CI], %	p-value	REID[95% CI], %	p-value
20 g/cm^2 Al	0.3	0.92 [0.31, 3.29]	6.36E-06	0.92 [0.53, 3.34]	5.50E-13	0.92 [0.56, 2.32]	6.32E-17
20 g/cm^2 PE	0.24	0.75 [0.25, 2.64]		0.75 [0.44, 2.71]		0.75 [0.46, 1.83]	

Table 6a. **Risk for Annual GCR at Solar Minimum for the 40-y Males Based on Average U.S. Population.** Shielding performance tests considers Q and space physics uncertainties alone ignoring uncertainties in DDREF, epidemiology data, and transfer model. Values in bold parentheses are not significant at the 95% CL. Results in bold italics are not significant at the 95% CI for a possible reduction compared to aluminum shielding.

Material		E (Sv)	REID[95% CI], %	p-value	REID[95% CI], %	p-value
			Q-uncorrelated Uncertainties		Q-correlated Uncertainties	
5 g/cm^2	Al	0.6	2.40 [1.32, 7.97]	-	2.40 [1.39, 5.59]	-
	PE	0.57	***2.25 [1.27, 7.60]***	***8.13E-02***	2.25 [1.33, 5.28]	2.46E-02
	Water	0.57	***2.28 [1.29, 7.58]***	***2.24E-01***	***2.28 [1.32, 5.29]***	***8.41E-02***
	Liquid H_2	0.47	1.87 [1.08, 6.41]	2.35E-16	1.87 [1.13, 4.43]	1.11E-22
	Epoxy	0.58	**2.30 [1.27, 7.65]**	***4.84E-01***	***2.30 [1.33, 5.43]***	***2.22E-01***
10 g/cm^2	Al	0.57	2.26 [1.27, 7.72]		2.26 [1.34, 5.30]	
	PE	0.52	2.05 [1.19, 7.10]	1.62E-03	2.05 [1.24, 4.84]	1.39E-04
	Water	0.53	***2.09 [1.21, 7.20]***	***1.01E-02***	2.09 [1.26, 4.93]	2.70E-03
	Liquid H_2	0.4	1.59 [0.99, 5.65]	7.78E-32	1.59 [1.01, 3.76]	1.06E-40
	Epoxy	0.53	***2.12 [1.23, 7.34]***	***7.81E-02***	2.12 [1.28, 5.06]	2.54E-02
20 g/cm^2	Al	0.53	2.10 [1.22, 7.28]		2.10 [1.27, 5.08]	
	PE	0.47	1.87 [1.13, 6.61]	1.03E-04	1.87 [1.18, 4.47]	4.81E-06
	Water	0.48	1.90 [1.15, 6.61]	8.89E-04	1.90 [1.20, 4.54]	8.09E-05
	Liquid H_2	0.36	1.40 [0.89, 4.99]	1.40E-44	1.40 [0.93, 3.33]	0.00E+00
	Epoxy	0.49	1.95 [1.18, 6.79]	2.68E-02	1.95 [1.21, 4.64]	4.98E-03
40 g/cm^2	Al	0.51	2.01 [1.22, 7.00]		2.01 [1.25, 4.81]	
	PE	0.46	1.80 [1.11, 6.31]	4.14E-05	1.80 [1.14, 4.32]	1.29E-06
	Water	0.46	1.81 [1.12, 6.42]	6.94E-05	1.81 [1.15, 4.32]	9.53E-06
	Liquid H_2	0.31	1.23 [0.79, 4.31]	0.00E+00	1.23 [0.81, 2.88]	0.00E+00
	Epoxy	0.48	***1.89 [1.17, 6.58]***	***5.11E-02***	1.89 [1.20, 4.54]	1.80E-02

Table 6b. **Risk for Annual GCR at Solar Minimum for a 40-y Male NS Population.** Shielding performance tests considers Q and space physics uncertainties alone ignoring uncertainties in DDREF, epidemiology data, and transfer model. Results in bold italics are not significant at the 95% CI for a possible reduction compared to aluminum shielding.

Material		E (Sv)	REID[95% CI], %	p-value	REID[95% CI], %	p-value
			Q-uncorrelated Uncertainties		Q-correlated Uncertainties	
5 g/cm^2	Al	0.6	1.87 [1.03, 6.25]	-	1.87 [1.08, 4.40]	-
	PE	0.57	***1.75 [0.99, 5.96]***	***8.44E-02***	1.75 [1.04, 4.13]	2.58E-02
	Water	0.57	***1.77 [1.00, 5.95]***	***2.33E-01***	***1.77 [1.03, 4.14]***	***8.60E-02***
	Liquid H_2	0.47	1.45 [0.84, 5.01]	1.13E-16	1.45 [0.88, 3.44]	3.77E-23
	Epoxy	0.58	***1.79 [0.99, 5.98]***	***4.89E-01***	***1.79 [1.03, 4.25]***	***2.20E-01***
10 g/cm^2	Al	0.57	1.76 [0.99, 6.05]	-	1.76 [1.04, 4.14]	-
	PE	0.52	1.59 [0.92, 5.55]	1.44E-03	1.59 [0.96, 3.78]	1.50E-04
	Water	0.53	1.62 [0.94, 5.64]	8.79E-03	1.62 [0.98, 3.85]	2.86E-03
	Liquid H_2	0.4	1.23 [0.76, 4.39]	1.58E-32	1.23 [0.78, 2.91]	1.66E-41
	Epoxy	0.53	***1.65 [0.95, 5.73]***	***7.03E-02***	1.65 [1.00, 3.96]	2.67E-02
20 g/cm^2	Al	0.53	1.63 [0.94, 5.70]	-	1.63 [0.99, 3.97]	-
	PE	0.47	1.45 [0.88, 5.14]	7.32E-05	1.45 [0.92, 3.49]	3.85E-06
	Water	0.48	1.48 [0.89, 5.15]	6.96E-04	1.48 [0.91, 3.54]	6.61E-05
	Liquid H_2	0.36	1.09 [0.69, 3.87]	2.80E-45	1.09 [0.70, 2.58]	0.00E+00
	Epoxy	0.49	1.52 [0.90, 5.31]	2.37E-02	1.52 [0.94, 3.62]	5.00E-03
40 g/cm^2	Al	0.51	1.56 [0.95, 5.45]	-	1.56 [0.97, 3.75]	-
	PE	0.46	1.40 [0.86, 4.91]	3.28E-05	1.40 [0.88, 3.35]	1.22E-06
	Water	0.46	1.40 [0.87, 4.99]	5.88E-05	1.40 [0.89, 3.37]	1.01E-05
	Liquid H_2	0.31	0.95 [0.61, 3.33]	0.00E+00	0.95 [0.63, 2.24]	0.00E+00
	Epoxy	0.48	1.47 [0.91, 5.14]	4.83E-02	1.47 [0.93, 3.54]	1.84E-02

Table 7a. Risk from August 1972 SPE and Annual GCR at Solar Maximum for 40-y Males Based on Average U.S. Population. Shielding performance tests considers Q and space physics uncertainties alone ignoring uncertainties in DDREF, epidemiology data and transfer model. Results in bold italics are not significant at the 95% CI for a possible reduction compared to aluminum shielding.

Material		E (Sv)	REID[95% CI], %	p-value	REID[95% CI], %	p-value
			Q-uncorrelated Uncertainties		Q-correlated Uncertainties	
5 g/cm^2	Al	0.69	2.70 [1.67, 11.33]	-	2.70 [1.74, 7.69]	-
	PE	0.54	2.15 [1.33, 8.83]	2.59E-18	2.15 [1.39, 6.00]	8.13E-24
	Water	0.57	2.25 [1.39, 9.12]	1.43E-12	2.25 [1.45, 6.16]	1.34E-16
	Liq H_2	0.3	1.17 [0.71, 4.58]	0.00E+00	1.17 [0.74, 3.08]	0.00E+00
	Epoxy	0.59	2.33 [1.44, 9.50]	1.82E-08	2.33 [1.51, 6.58]	2.71E-11
10 g/cm^2	Al	0.43	1.70 [1.01, 6.73]		1.70 [1.05, 4.55]	-
	PE	0.33	1.31 [0.78, 5.04]	1.65E-21	1.31 [0.81, 3.36]	3.21E-27
	Water	0.35	1.37 [0.81, 5.32]	4.71E-15	1.37 [0.85, 3.52]	2.54E-19
	Liq H_2	0.19	0.77 [0.46, 2.80]	0.00E+00	0.77 [0.48, 1.86]	0.00E+00
	Epoxy	0.36	1.44 [0.85, 5.55]	8.37E-10	1.44 [0.89, 3.75]	1.49E-12
20 g/cm^2	Al	0.3	1.18 [0.68, 4.28]		1.18 [0.72, 2.97]	-
	PE	0.24	0.96 [0.57, 3.48]	3.00E-12	0.96 [0.60, 2.36]	2.44E-16
	Water	0.25	0.99 [0.59, 3.54]	1.16E-09	0.99 [0.61, 2.43]	9.25E-13
	Liq H_2	0.16	0.65 [0.40, 2.32]	0.00E+00	0.65 [0.41, 1.55]	0.00E+00
	Epoxy	0.26	1.04 [0.60, 3.71]	7.59E-06	1.04 [0.63, 2.54]	1.45E-07
40 g/cm^2	Al	0.26	1.05 [0.61, 3.69]		1.05 [0.64, 2.56]	-
	PE	0.23	0.91 [0.55, 3.19]	3.12E-08	0.91 [0.57, 2.19]	5.14E-10
	Water	0.23	0.92 [0.55, 3.27]	2.56E-07	0.92 [0.57, 2.21]	2.94E-09
	Liq H_2	0.15	0.59 [0.37, 2.05]	0.00E+00	0.59 [0.38, 1.38]	0.00E+00
	Epoxy	0.24	0.97 [0.58, 3.38]	4.17E-03	0.97 [0.60, 2.35]	5.74E-04

Table 7b. Risk from August 1972 SPE and Annual GCR at Solar Maximum for 40-y Males Based on NS Population. Shielding performance tests considers Q and space physics uncertainties alone ignoring uncertainties in DDREF, epidemiology data, and transfer model. Results in bold italics are not significant at the 95% CI for a possible reduction compared to aluminum shielding.

Material		E (Sv)	REID[95% CI], %	p-value	REID[95% CI], %	p-value
			Q-uncorrelated Uncertainties		Q-correlated Uncertainties	
5 g/cm^2	Al	0.69	2.17 [1.34, 9.13]	-	2.17 [1.40, 6.24]	-
	PE	0.54	1.71 [1.06, 7.04]	5.06E-19	1.71 [1.11, 4.81]	2.02E-25
	Water	0.57	1.80 [1.11, 7.31]	3.13E-13	1.80 [1.16, 4.94]	7.37E-18
	Liq H_2	0.3	0.92 [0.56, 3.60]	0.00E+00	0.92 [0.58, 2.41]	0.00E+00
	Epoxy	0.59	1.87 [1.15, 7.63]	3.30E-09	1.87 [1.21, 5.29]	3.09E-12
10 g/cm^2	Al	0.43	1.34 [0.79, 5.31]		1.34 [0.83, 3.59]	-
	PE	0.33	1.03 [0.61, 3.96]	8.83E-23	1.03 [0.64, 2.65]	1.72E-28
	Water	0.35	1.08 [0.64, 4.17]	5.65E-16	1.08 [0.67, 2.76]	1.37E-20
	Liq H_2	0.19	0.59 [0.36, 2.17]	0.00E+00	0.59 [0.38, 1.44]	0.00E+00
	Epoxy	0.36	1.13 [0.67, 4.37]	2.82E-10	1.13 [0.70, 2.96]	3.86E-13
20 g/cm^2	Al	0.3	0.92 [0.53, 3.34]		0.92 [0.56, 2.32]	-
	PE	0.24	0.75 [0.44, 2.71]	5.50E-13	0.75 [0.46, 1.83]	6.32E-17
	Water	0.25	0.77 [0.45, 2.74]	2.72E-10	0.77 [0.48, 1.89]	3.07E-13
	Liq H_2	0.16	0.50 [0.31, 1.79]	0.00E+00	0.50 [0.32, 1.20]	0.00E+00
	Epoxy	0.26	0.81 [0.47, 2.89]	7.62E-06	0.81 [0.49, 1.97]	7.24E-08
40 g/cm^2	Al	0.26	0.82 [0.47, 2.87]		0.82 [0.49, 1.98]	-
	PE	0.23	0.70 [0.42, 2.48]	3.33E-08	0.70 [0.44, 1.70]	4.51E-10
	Water	0.23	0.71 [0.43, 2.54]	2.64E-07	0.71 [0.44, 1.71]	3.15E-09
	Liq H_2	0.15	0.45 [0.29, 1.59]	0.00E+00	0.45 [0.29, 1.07]	0.00E+00
	Epoxy	0.24	0.75 [0.45, 2.62]	3.54E-03	0.75 [0.46, 1.83]	5.06E-04

Table 8a. **Results for the Two-layer Shielding System for the Same Solar Min Condition of Table 6a.** Results in bold italics are not significant at the 95% CI for a possible reduction compared to aluminum shielding.

Material			E (Sv)	Q-Uncorrelated Uncertainties		Q-correlated Uncertainties	
1st layer	2nd layer			REID[95% CI], %	p-value	REID[95% CI], %	p-value
10 g/cm^2 Al	5 g/cm^2	Al	0.55	2.16 [1.25, 7.46]	-	2.16 [1.31, 5.14]	-
		PE	0.52	***2.07 [1.20, 7.05]***	***2.56E-01***	***2.07 [1.25, 4.94]***	***1.61E-01***
		Water	0.53	***2.09 [1.21, 7.08]***	***4.64E-01***	***2.09 [1.26, 4.95]***	***3.27E-01***
		Liquid H_2	0.45	1.79 [1.08, 6.19]	7.07E-11	1.79 [1.13, 4.27]	8.40E-15
		Epoxy	0.53	***2.11 [1.22, 7.23]***	***7.62E-01***	***2.11 [1.27, 4.94]***	***5.20E-01***
	10 g/cm^2	Al	0.53	2.10 [1.22, 7.25]	-	2.10 [1.27, 4.99]	-
		PE	0.5	1.96 [1.16, 6.89]	4.00E-02	1.96 [1.21, 4.71]	6.87E-03
		Water	0.5	***1.98 [1.17, 7.00]***	***1.04E-01***	1.98 [1.23, 4.76]	2.73E-02
		Liquid H_2	0.4	1.59 [0.99, 5.64]	5.29E-23	1.59 [1.03, 3.78]	3.24E-30
		Epoxy	0.51	***2.01 [1.19, 7.08]***	***3.79E-01***	***2.01 [1.25, 4.86]***	***1.08E-01***
	20 g/cm^2	Al	0.52	2.04 [1.21, 7.08]	-	2.04 [1.26, 4.81]	-
		PE	0.47	1.86 [1.13, 6.59]	1.31E-03	1.86 [1.18, 4.49]	2.19E-04
		Water	0.48	1.88 [1.14, 6.56]	5.42E-03	1.88 [1.19, 4.43]	9.94E-04
		Liquid H_2	0.36	1.42 [0.90, 4.89]	1.50E-38	1.42 [0.94, 3.34]	0.00E+00
		Epoxy	0.49	***1.93 [1.17, 6.78]***	***1.13E-01***	***1.93 [1.22, 4.71]***	***5.05E-02***
	40 g/cm^2	Al	0.51	2.01 [1.22, 7.07]	-	2.01 [1.27, 4.85]	-
		PE	0.46	1.81 [1.12, 6.34]	1.56E-04	1.81 [1.15, 4.37]	7.54E-06
		Water	0.46	1.82 [1.13, 6.35]	2.83E-04	1.82 [1.15, 4.37]	5.15E-05
		Liquid H_2	0.31	1.24 [0.80, 4.28]	0.00E+00	1.24 [0.82, 2.93]	0.00E+00
		Epoxy	0.48	***1.90 [1.15, 6.61]***	***7.66E-02***	1.90 [1.20, 4.51]	3.73E-02

Table 8b. **Results for the Two-layer Shielding System for the Solar Min Condition of Table 6b.** Results in bold italics are not significant at the 95% CI for a possible reduction compared to aluminum shielding.

Material			E (Sv)	Q-uncorrelated Uncertainties		Q-correlated Uncertainties	
1st layer	2nd layer			REID[95% CI], %	p-value	REID[95% CI], %	p-value
10 g/cm^2 Al	5 g/cm^2	Al	0.55	1.68 [0.97, 5.82]	-	1.68 [1.02, 4.01]	-
		PE	0.52	***1.61 [0.93, 5.52]***	***2.60E-01***	***1.61 [0.97, 3.86]***	***1.63E-01***
		Water	0.53	***1.62 [0.94, 5.52]***	***4.71E-01***	***1.62 [0.98, 3.87]***	***3.36E-01***
		Liquid H_2	0.45	1.39 [0.84, 4.83]	3.92E-11	1.39 [0.86, 3.33]	4.99E-15
		Epoxy	0.53	***1.63 [0.94, 5.66]***	***7.60E-01***	***1.63 [0.99, 3.86]***	***5.25E-01***
	10 g/cm^2	Al	0.53	1.63 [0.94, 5.68]	-	1.63 [0.99, 3.90]	-
		PE	0.5	1.52 [0.90, 5.39]	4.11E-02	1.52 [0.94, 3.67]	5.53E-03
		Water	0.5	***1.54 [0.91, 5.47]***	***7.99E-02***	1.54 [0.95, 3.71]	2.53E-02
		Liquid H_2	0.4	1.23 [0.76, 4.38]	7.17E-23	1.23 [0.80, 2.92]	5.19E-30
		Epoxy	0.51	***1.56 [0.92, 5.54]***	***3.69E-01***	***1.56 [0.97, 3.79]***	***1.10E-01***
	20 g/cm^2	Al	0.52	1.58 [0.94, 5.54]	-	1.58 [0.98, 3.75]	-
		PE	0.47	1.44 [0.87, 5.13]	1.23E-03	1.44 [0.91, 3.50]	1.85E-04
		Water	0.48	1.46 [0.88, 5.12]	5.60E-03	1.46 [0.92, 3.46]	1.03E-03
		Liquid H_2	0.36	1.10 [0.70, 3.80]	1.57E-39	1.10 [0.73, 2.60]	0.00E+00
		Epoxy	0.49	***1.50 [0.91, 5.30]***	***1.15E-01***	***1.50 [0.95, 3.67]***	***5.20E-02***
	40 g/cm^2	Al	0.51	1.56 [0.94, 5.52]	-	1.56 [0.99, 3.78]	-
		PE	0.46	1.40 [0.87, 4.93]	1.43E-04	1.40 [0.89, 3.41]	7.52E-06
		Water	0.46	1.41 [0.87, 4.94]	2.15E-04	1.41 [0.89, 3.39]	4.08E-05
		Liquid H_2	0.31	0.96 [0.60, 3.32]	0.00E+00	0.96 [0.63, 2.28]	0.00E+00
		Epoxy	0.48	***1.47 [0.89, 5.16]***	***6.16E-02***	1.47 [0.93, 3.52]	3.19E-02

Table 9a. Results for the Two-layer Shielding System for the Solar Max Conditions of Table 7a. Results in bold italics are not significant at the 95% CI for a possible reduction compared to aluminum shielding.

Material			E (Sv)	Q-uncorrelated Uncertainties		Q-correlated Uncertainties	
1st layer	2nd layer			REID[95% CI], %	p-value	REID[95% CI], %	p-value
10 g/cm^2 Al	5 g/cm^2	Al	0.34	1.34 [0.77, 5.00]	-	1.34 [0.81, 3.38]	-
		PE	0.31	1.22 [0.70, 4.45]	1.87E-03	1.22 [0.74, 3.08]	3.52E-04
		Water	0.31	1.24 [0.72, 4.52]	1.91E-02	1.24 [0.75, 3.12]	2.30E-03
		Liq H_2	0.24	0.94 [0.56, 3.38]	3.21E-33	0.94 [0.58, 2.32]	1.49E-43
		Epoxy	0.32	***1.26 [0.73, 4.64]***	***8.50E-02***	1.26 [0.76, 3.13]	2.25E-02
	10 g/cm^2	Al	0.3	1.18 [0.68, 4.28]	-	1.18 [0.72, 2.92]	-
		PE	0.26	1.05 [0.61, 3.80]	4.81E-05	1.05 [0.63, 2.59]	1.05E-06
		Water	0.27	1.07 [0.62, 3.93]	7.93E-04	1.07 [0.65, 2.66]	6.26E-05
		Liq H_2	0.2	0.78 [0.47, 2.77]	0.00E+00	0.78 [0.49, 1.86]	0.00E+00
		Epoxy	0.27	1.10 [0.63, 3.97]	2.23E-02	1.10 [0.66, 2.72]	2.91E-03
	20 g/cm^2	Al	0.27	1.08 [0.62, 3.81]	-	1.08 [0.65, 2.59]	-
		PE	0.24	0.95 [0.56, 3.39]	3.97E-06	0.95 [0.59, 2.31]	1.15E-07
		Water	0.24	0.96 [0.57, 3.39]	4.17E-05	0.96 [0.59, 2.31]	1.28E-06
		Liq H_2	0.17	0.68 [0.42, 2.36]	0.00E+00	0.68 [0.44, 1.62]	0.00E+00
		Epoxy	0.25	0.99 [0.59, 3.52]	1.30E-02	0.99 [0.61, 2.45]	2.61E-03
	40 g/cm^2	Al	0.26	1.06 [0.62, 3.74]	-	1.06 [0.65, 2.58]	-
		PE	0.23	0.93 [0.56, 3.27]	3.66E-06	0.93 [0.59, 2.26]	4.46E-08
		Water	0.23	0.93 [0.56, 3.28]	7.22E-06	0.93 [0.58, 2.25]	6.12E-07
		Liq H_2	0.15	0.60 [0.38, 2.10]	0.00E+00	0.60 [0.39, 1.44]	0.00E+00
		Epoxy	0.25	0.98 [0.58, 3.43]	1.22E-02	0.98 [0.61, 2.35]	4.17E-03

Table 9b. **Results for the Two-layer Shielding System for the Solar Max Conditions of Table 7b.** Results in bold italics are not significant at the 95% CI for a possible reduction compared to aluminum shielding.

Material			E (Sv)	Q-uncorrelated Uncertainties		Q-correlated Uncertainties	
1st layer	2nd layer			REID[95% CI], %	p-value	REID[95% CI], %	p-value
10 g/cm^2 Al	5 g/cm^2	Al	0.34	1.05 [0.60, 3.90]	-	1.05 [0.63, 2.64]	-
		PE	0.31	0.95 [0.55, 3.48]	1.29E-03	0.95 [0.58, 2.40]	2.98E-04
		Water	0.31	0.97 [0.56, 3.54]	1.51E-02	0.97 [0.59, 2.44]	1.74E-03
		Liq H_2	0.24	0.73 [0.43, 2.62]	5.24E-35	0.73 [0.45, 1.80]	0.00E+00
		Epoxy	0.32	***0.98 [0.57, 3.64]***	***6.90E-02***	0.98 [0.60, 2.44]	1.71E-02
	10 g/cm^2	Al	0.3	0.92 [0.53, 3.33]	-	0.92 [0.56, 2.27]	-
		PE	0.26	0.81 [0.47, 2.96]	3.77E-05	0.81 [0.49, 2.01]	8.78E-07
		Water	0.27	0.83 [0.48, 3.05]	8.17E-04	0.83 [0.50, 2.07]	4.34E-05
		Liq H_2	0.2	0.60 [0.36, 2.15]	0.00E+00	0.60 [0.38, 1.45]	0.00E+00
		Epoxy	0.27	0.85 [0.49, 3.10]	1.53E-02	0.85 [0.52, 2.13]	2.81E-03
	20 g/cm^2	Al	0.27	0.84 [0.48, 2.96]	-	0.84 [0.51, 2.01]	-
		PE	0.24	0.73 [0.43, 2.63]	2.67E-06	0.73 [0.45, 1.79]	7.20E-08
		Water	0.24	0.74 [0.44, 2.63]	4.30E-05	0.74 [0.46, 1.79]	1.37E-06
		Liq H_2	0.17	0.53 [0.33, 1.82]	0.00E+00	0.53 [0.34, 1.25]	0.00E+00
		Epoxy	0.25	0.77 [0.46, 2.74]	8.33E-03	0.77 [0.48, 1.91]	1.59E-03
	40 g/cm^2	Al	0.26	0.82 [0.48, 2.91]	-	0.82 [0.51, 1.99]	-
		PE	0.23	0.72 [0.43, 2.53]	3.79E-06	0.72 [0.45, 1.75]	4.74E-08
		Water	0.23	0.72 [0.44, 2.55]	7.47E-06	0.72 [0.45, 1.74]	6.57E-07
		Liq H_2	0.15	0.47 [0.30, 1.62]	0.00E+00	0.47 [0.30, 1.11]	0.00E+00
		Epoxy	0.25	0.76 [0.45, 2.66]	1.23E-02	0.76 [0.47, 1.83]	4.33E-03

6.0 References

Badhwar GD, O'Neill PM. An improved model of GCR for space exploration missions. Nucl. Tracks Radiat. Meas 20: 403-410; 1992.

Barcellos-Hoff MH, Park C, Wright EG. Radiation and the microenvironment – tumorigenesis and therapy. Nat Rev Cancer 5:867-875; 2005.

Barkas H. *Nuclear Research Emulsions.* Academic Press Inc., New York. Vol. 1, Chap. 9, p. 371, 1963.

BEIR VII, National Academy of Sciences Committee on the Biological Effects of Radiation, Health Risks From Exposure to Low Levels of Ionizing Radiation. Washington DC: National Academy of Sciences Press; 2006.

Billings MP, Yucker WR, Heckman BR. Body self-shielding data analysis. Huntington Beach, Calif: McDonald Douglas Astronautics Company West; 1973. MDC-G4131.

CDC, *2005 Cancer incidence* – United States Cancer Statistics: 1999 - 2005 Incidence, WONDER On-line Database. United States Department of Health and Human Services, Centers for Disease Control and Prevention and National Cancer Institute; August 2008. Accessed at http://wonder.cdc.gov/cancer-v2005.html on Apr 23, 2010. *CDC, 2005 Cancer mortality* – United States Cancer Statistics: 1999 - 2005 Mortality, WONDER On-line Database. United States Department of Health and Human Services, Centers for Disease Control and Prevention; August 2008. Accessed at http://wonder.cdc.gov/CancerMort-v2005.html on Apr 23, 2010.

CDC-MMWR, Morbidity Weekly Report. Center of Disease Control 57:1226-1228; 2008.

CDC, United States Department of Health and Human Services, How Tobacco Smoke Causes Disease: the Biology and Behavioral Basis for Smoking-Attributable Disease: A Report of the Surgeon General. Center for Disease Control, Atlanta GA, 2010.

Cucinotta FA and Dubey R R. Alpha Cluster Description of Excitation Energies in ^{12}C (^{12}C, 3α) X at 2.1 GeV. Physical Review C 50: 979-984; 1994

Cucinotta FA, Townsend LW, Wilson JW, Shinn JL, Badhwar GD, and RR Dubey. Light ion component of the galactic cosmic rays: nuclear interactions and transport theory. Adv Space Res 17: 77-86; 1995.

Cucinotta FA, Nikjoo H, and Goodhead DT. Comment on the Effects of Delta-Rays on the Number of Particle-Track Transversals Per Cell in Laboratory and Space Exposures. Radiat Res 150: 115-119; 1998.

Cucinotta FA, Kim MY, and Ren L. Evaluating shielding effectiveness for reducing space radiation cancer risks. Radiat Meas 41:1173-1185; 2006.

Cucinotta FA, Durante M. Cancer risk from exposure to galactic cosmic rays: implications for space exploration by human beings. The Lancet Onc 7: 431-435; 2006.

Cucinotta FA, Kim MY, Schneider SI, Hassler DM. Description of light ion production cross sections and fluxes on the Mars surface using the QMSFRG model. Radiat Environ Biophys 46: 101-106; 2007.

Cucinotta FA, Chappell LJ, Non-targeted effects and the dose response for heavy ion tumor formation. Mutat Res 687:49-53; 2010.

Cucinotta FA, Chappell L. Updates to astronaut radiation limits: radiation risks for never-smokers. Radiat Res 176:102-114; 2011.

Cucinotta FA, Kim MY Chappell L. Space radiation cancer risk projections and uncertainties-2010. NASA TP 2011-216155; 2011.

Cucinotta FA, Chappell LJ, Kim MY, and Wang M. Radiation Carcinogenesis Risk Assessments for Never-Smokers. Health Phys (in press), 2012.

DHHS (2002). U.S. Department of Health and Human Services. "42 CFR Part 81: 7868 Guidelines for determining the probability of causation under the Energy Employees Occupational Illness Compensation Program Act of 2000, Final Rule," 67 FR 22296–22314 (U.S. Government Printing Office, Washington).

Durante M, Cucinotta FA. Heavy ion carcinogenesis and human space exploration. Nat Rev Cancer 8:465-472; 2008.

Durante M, Cucinotta FA. Physical Basis of radiation protection in space travel. Rev Mod Phys 83, 1245-1281; 2011.

Elandt-Johnson RC, Johnson N. Survival Models and Data Analysis. Wiley, New York, 1999.

Furukawa K, Preston DL, Lonn S, Funamoto S, Yonehara S, Takeshi M, et al. Radiation and smoking effects on lung cancer incidence among atomic bomb survivors. Radiat Res 174:72-82; 2010.

Hu S, Kim MY, McClellan E, and Cucinotta FA. Modeling the acute health effects to astronauts from exposure to solar particle events. Health Phys 96: 465-476; 2009.

ICRP, *1990 Recommendations of the International Commission on Radiological Protection*. ICRP Publication 60, Pergamon Press, Oxford, 1990.

ICRP, *Relative Biological Effectiveness (RBE), Quality Factor (Q), and Radiation Weighting Factor (w_R).* ICRP Publication 103. International Commission on Radiation Protection, Pergamon, 2003.

Kim MY, and Cucinotta: Probabilistic Assessment of Radiation Risk from Solar Particle Events. Proceedings: SP-662, Huguette Lacoste-Francis, Editor, ESA Communication and Production Office, 3rd IAASS Conference, Rome, Italy, October 23, 2008.

Kim MY, Hayat ML, Feiveson AH, and Cucinotta FA. Using high-energy proton fluence to improve risk prediction for consequences of solar particle events. Adv Space Res 44: 1428-1432; 2009.

NCRP, *Uncertainties in Fatal Cancer Risk Estimates Used in Radiation Protection*, National Council on Radiation Protection and Measurements Report 126: Bethesda MD, 1997.

NCRP. *Recommendations of Dose Limits for Low Earth Orbit*. National Council on Radiation Protection and Measurements Report 132: Bethesda MD; 2000.

NCRP, *Information Needed to Make Radiation Protection Recommendations for Space Missions Beyond Low-Earth Orbit*. National Council on Radiation Protection and Measurements Report No. 153**:** Bethesda MD, 2006.

NIH. *Report of the NCI-CDC Working Group to Revise the 1985 NIH Radioepidemiological Tables*. NIH Publication No. 03-5387; 2003.

Pawel D, Preston DL, Pierce D, Cologne J. Improved estimates of cancer site-specific risks for A-bomb survivors. Radiat Res 169: 87-98, 2008.

Preston DL, Ron E, Tokuoka S, Funamota S, Nishi N, Soda M, Mabuchi K, et al. Solid cancer incidence in atomic bomb survivors: 1958-1998. Radiat Res 168:1-64; 2007.

Schimmerling W, Wilson JW, Cucinotta FA, Kim MH. Requirements for simulating space radiations with particle accelerators. In: Risk Evaluation of Cosmic- Ray Exposure in Long-Term Manned Space Mission (K. Fujitaka, H. Majima, K. Ando, H. Yasuda, and M. Susuki, Eds., Kodansha Scientific Ltd., Tokyo) 1-16, 1999.

SEER, Surveillance, Epidemiology, and End Results: Cancer Statistics Review, 2005. Cancer Surveillance Research Program, National Cancer Institute: Bethesda MD; 2006.

Storer JB, Mitchell TJ, Fry RJ. Extrapolation of the relative risk of radiogenic neoplasms across mouse strains and to man. Radiat Res 113: 331-353; 1988.

Thun MJ, Day-Lally C, Calle E, Flanders W, Heath C. Excess mortality among cigarette smokers: changes in a 20-year interval. Am J Public Health 85:1223–1230; 1995.

Thun MJ, Hannan LM, Adams-Campbell LL, Boffetta P, Buring JE, Feskanich D, et al. Lung cancer occurrence in never-smokers: an analysis of 13 cohorts and 22 cancer registry studies. PLoS Med 5:1357-1371; 2008

UNSCEAR, United Nations Scientific Committee on the Effects of Atomic Radiation, Sources and Effects of Ionizing Radiation. UNSCEAR 2006 Report to the General Assembly, with Scientific Annexes. New York: United Nations; 2008.

Weil MM, Bedford JS, Bielefeldt-Ohmann H, Ray AF, Gernik PC, Ehrhart EJ, Falgren CM, Hailu F, Battaglia CLR, Charles C, Callan MA, Ullrich RL. Incidence of acute myeloid leukemia and hepatocellular carcinoma in mice irradiated with 1 GeV/nucleon ^{56}Fe ions. Radiat Res 172**:**213-219; 2009.

Wilson JW, Townsend LW, Schimmerling W, Khandelwal GS, Khan F, Nealy JE, Cucinotta FA, Simonsen LC, Shinn JL, Norbury JW. Transport methods and interactions for space radiations. NASA RP 1257, 1991.

Wilson JW, Townsend LW, Shinn JL, Cucinotta FA, Costen RC, Badavi FF, Lamkin SL. Galactic cosmic ray transport methods, past, present, and future. Adv Space Res 10: 841-852; 1994.

Wilson JW, Kim M, Schimmerling W, Badavi F, Thibeault S, Cucinotta FA, Shinn J, and Kiefer R,1995, Issues in space radiation protection. Health Phys 68: 50-58; 1995.

Wilson JW, Cucinotta FA, Miller J, Shinn JL, Thibeault SA, Singleterry RC, Simonsen LC, and Kim MH. “Approaches and issues related to shield material design to protect astronauts from space radiation”, Materials and Design 22: 541-554; 2001.

REPORT DOCUMENTATION PAGE

Form Approved
OMB No. 0704-0188

1. AGENCY USE ONLY *(Leave Blank)*	2. REPORT DATE	3. REPORT TYPE AND DATES COVERED
	May 2012	NASA Technical Memorandum

4. TITLE AND SUBTITLE
Evaluating Shielding Approaches to Reduce Space Radiation Cancer Risks

5. FUNDING NUMBERS

6. AUTHOR(S)
Francis A. Cucinotta; Myung-Hee Y. Kim; Lori J. Chappell

7. PERFORMING ORGANIZATION NAME(S) AND ADDRESS(ES)
Lyndon B. Johnson Space Center
Houston, Texas 77058

8. PERFORMING ORGANIZATION REPORT NUMBERS
S-1123

9. SPONSORING/MONITORING AGENCY NAME(S) AND ADDRESS(ES)
National Aeronautics and Space Administration
Washington, DC 20546-0001

10. SPONSORING/MONITORING AGENCY REPORT NUMBER
TM-2012-217361

11. SUPPLEMENTARY NOTES

12a. DISTRIBUTION/AVAILABILITY STATEMENT
Available from the NASA Center for AeroSpace Information (CASI)
7121 Standard
Hanover, MD 21076-1320 Category: 52

12b. DISTRIBUTION CODE

13. ABSTRACT *(Maximum 200 words)*

It remains a challenge for NASA to protect astronauts from galactic cosmic rays (GCRs) and solar particle events (SPEs) during long-duration missions. Shielding of SPEs is understood scientifically, which has led to readily available technology solutions, with optimization of specific designs to minimize launch mass. However, high-energies and secondary radiation of GCR limit most shielding approaches to small reductions from a baseline shielding configuration. We make a revised assessment of shielding materials performance based on newly defined NASA track structure dependent radiation quality factors, and most recent uncertainty analysis of space radiation cancer risks. Comparisons of liquid hydrogen, polyethylene, water, and epoxy shielding to aluminum for one-layer configurations with depths of 5 to 40 g/cm2, or two-layer configurations with an outer 10 g/cm2 aluminum layer, are considered. Statistically significant improvements in GCR risk reduction relative to aluminum shielding can be obtained with hydrocarbon materials with significant hydrogen content. Comparisons for several spacecraft designs for certain radiation environments are discussed. Liquid hydrogen remains the optimal shielding material; however, its performance can be overestimated if secondary radiation produced in tissue or the vessel containing the hydrogen are not considered. Nevertheless, developing new multifunctional shielding materials with higher hydrogen content compared to polyethylene is advocated.

14. SUBJECT TERMS	15. NUMBER OF PAGES	16. PRICE CODE
long duration space flight; shielding; radiation shielding; galactic cosmic rays; radiation effects; cancer;	46	

17. SECURITY CLASSIFICATION OF REPORT	18. SECURITY CLASSIFICATION OF THIS PAGE	19. SECURITY CLASSIFICATION OF ABSTRACT	20. LIMITATION OF ABSTRACT
Unclassified	Unclassified	Unclassified	Unlimited

Standard Form 298 (Rev Feb 89) (MS Word Mar 97) NSN 7540-01-280-5500
Prescribed by ANSI Std. 239-18
298-102